Quartz-kyanite pods in the Tusas Mountains, northern New Mexico: A sheared and metamorphosed fossil hydrothermal system in the Vadito Group metarhyolite

Mary C. Simmons, Karl E. Karlstrom, Michael W. Williams, and Toti E. Larson, 2011, pp. 359-378
in:
Geology of the Tusas Mountains and Ojo Caliente, Author Koning, Daniel J.; Karlstrom, Karl E.; Kelley, Shari A.; Lueth, Virgil W.; Aby, Scott B., New Mexico Geological Society 62nd Annual Fall Field Conference Guidebook, 418 p.

This page is intentionally left blank to maintain order of facing pages.

QUARTZ-KYANITE PODS IN THE TUSAS MOUNTAINS, NORTHERN NEW MEXICO: A SHEARED AND METAMORPHOSED FOSSIL HYDROTHERMAL SYSTEM IN THE VADITO GROUP METARHYOLITE

MARY C. SIMMONS[1], KARL E. KARLSTROM[1], MICHAEL W. WILLIAMS[2], AND TOTI E. LARSON[3]
[1]Department of Earth and Planetary Sciences, University of New Mexico, Albuquerque, NM, 87131, kyanitequeen@gmail.com
[2]Department of Geosciences, University of Massachusetts, Amherst, MA, 01003
[3]Geology and Geochemical Research Lab, Los Alamos National Laboratory, Los Alamos, NM 87545

Abstract—Lenses and pods or knobs of quartz-kyanite schist occur within a stratiform, map-scale white mica schist horizon in the 1.7 Ga. Vadito Group metarhyolite in the Tusas Mountains of northern New Mexico. Unusually high Al-bulk compositions in the large quartz-kyanite pods are likely the result multiple alteration processes that operated during the long history of volcanism and four episodes of deformation and metamorphism. Geochemical data collected in sampling traverses across the Vadito Group metarhyolite through the quartz-kyanite pods and sericite schist layer, combined with mineral textures and map patterns, provided the means to evaluate the origin and tectonic evolution of these unusual rocks. Geochemical trends from the sampling traverses show symmetrical depletion of Ca, Na, K, Fe, and enrichment of Si toward the centers of the quartz-kyanite pods, indicating alteration typical of shear zones and hydrothermal zones, but atypical of weathering profiles. Map patterns, geochemistry and mineral textures suggest the aligned quartz-kyanite pods may be the metamorphosed remnants of a hydrothermal alteration zone that was active during Vadito Group volcanism. We envision that hot acidic fluids migrated along fractures, altering rhyolite host rocks, and producing lenses and zones of clay and other minerals including pyrophyllite, chloritoid and possibly andalusite and staurolite. Weakened hydrothermally altered zones (represented by the quartz-kyanite pods) were linked together into a map-scale white-mica-rich S_1 shear zone during D_1 metamorphism, causing additional metasomatic leaching of mobile elements (e.g. Ca, Na, Fe, K) that enhanced the concentration of silica and aluminum in this zone. Quartz-kyanite oxygen isotope thermometry on two distinct varieties of kyanite, produced δ18O values of 7.0 and 7.5 per mil, corresponding to temperatures of formation of 530ºC and 590ºC, and correlate with peak metamorphic conditions. Light δ18O values may indicate an early hydrothermal system that acted on these rocks prior to metamorphism. We hypothesize a P-T path for the quartz-kyanite pods that began with sub-surface (1-2 km) hydrothermal alteration of Vadito Group metarhyolite and the production of kaolinite at temperatures less than <300ºC, and ended with peak metamorphism within the kyanite stability field during D_2, at conditions of around 500ºC and 400 MPa.

INTRODUCTION

Paleoproterozoic quartz-kyanite schist pods, consisting of up to 25 weight % Al_2O_3 and 40% kyanite (Schreyer and Chinner, 1966) crop out in the Tusas Mountains of northern New Mexico as lenticular pods and ridges up to 40 meters high (Fig. 1) within a stratiform, map-scale white-mica schist layer. The quartz-kyanite/white mica (e.g. paragonite, pyrophyllite) schist horizon is 0-20 meter thick, sub-parallel to folded stratigraphic contacts, and is mappable for about 5 kilometers. This compositionally unusual layer is part of the 1.7 Ga Vadito Group, an assemblage of metamorphosed rhyolite tuff and flows, micaceous quartzite, and metaconglomerate. Kyanite is present in sufficient volume for commercially exploitation: 1500 tons were mined in the 1920's (Bingler, 1965).

The unusually high Al-bulk composition of the large quartz-kyanite pods has been attributed to several processes. Previous studies have proposed metasomatic processes, where fluid transport was controlled by active shear zones (Gresens, 1971, 1972, 1976; Gresens and Stensrud, 1974a, 1974b); or K-rich pegmatitic hydrothermal alteration and Al-Si metasomatism (Barker, 1958). Corey (1960) hypothesized that the quartz-kyanite pods are the result of metamorphic differentiation of silt lenses, although this layer does not have the composition of any known sedimentary rock. Similar deposits of kyanite at Henry's Knob in the Carolina Slate Belt have alternately been interpreted to be of metasedimentary (Feiss et al.,1991) or hydrothermal (Smith and Newcome, 1951) origin.

This paper summarizes results of field, geochemical, and microstructural analyses aimed at understanding the origins of the unusual high Al-bulk compositions in the quartz-kyanite pods, and the type(s) and the timing of kyanite (and other metamorphic mineral) growth, relative to fold and fabric generations. We hypothesize that early hydrothermal alteration took place during Vadito Group volcanism, locally leaching and altering rhyolitic rocks to clay and clay-mica minerals. This altered zone subsequently experienced several episodes of deformation and metamorphism between ~1.65 Ga and 1.4 Ga, enhancing the concentration of Al and Si.

GEOLOGIC SETTING AND ROCK UNITS

The quartz-kyanite rocks are part of a large region of metamorphosed volcanic, metasedimentary, and plutonic rocks (Fig. 2a) that formed during the collision of island arcs and microcontinents with the Wyoming craton between 1.8 and 1.6 Ga (Bowring and Karlstrom, 1990). Multiple episodes of regional deformation occurred between 1.65 Ga and 1.4 Ga, resulting in a complex pattern of refolded folds, which have been difficult to correlate between the northern, central and southern Tusas Mountains (Williams, 1991). All rocks within the map area exhibit a pervasive NW-striking, SW-dipping (S_2) foliation that is axial planar

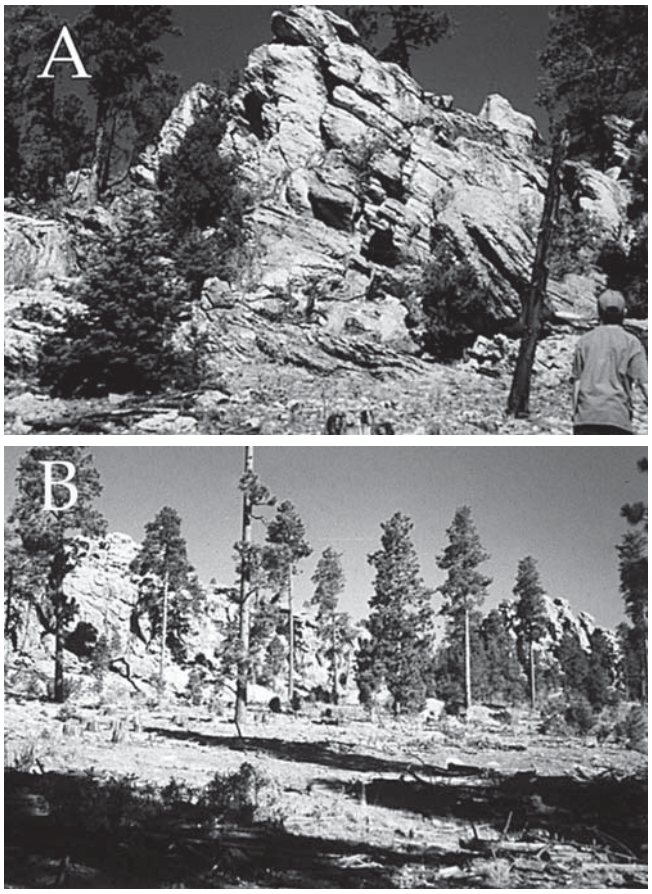

FIGURE 1. Photographs of quartz-kyanite knobs: (A) Kyanite Deposit #1; (B) Big Rock Kyanite Deposit. See Figure 2 for locations.

to map scale (F_2) folds. Simmons (1999) and Aby et al. (2010) mapped the area in detail.

The quartz-kyanite rocks form a discontinuous string of lenticular knobs or pods (Fig. 2b) that occur within the voluminous metarhyolite of the Vadito Group, a heterogeneous stack of metamorphosed rhyolite tuff and flows, micaceous quartzite, and metaconglomerate (Fig. 3). The quartz-kyanite pods are mappable within a continuous white mica-rich layer that roughly parallels folded stratigraphy. In this paper, we use the historical designation (e.g. Corey, 1960; Shreyer and Chinner, 1966) of sericite and sericite schist to refer to white mica, which is likely to be composed of paragonite, muscovite and possibly pyrophyllite. The pod assemblage is primarily quartz + kyanite, with sericite, minor coarser-grained muscovite, staurolite, chloritoid, magnetite, hematite, +/- tourmaline and relict quartz phenocrysts similar to those found in the host metarhyolite schist.

Kyanite occurs in several forms (Figs. 4a,b,c): (1) aligned in a fine-grained early mylonitic fabric; (2) in radial habit or within lumps of sericite that may be pseudomorphs after pyrophyllite and andalusite; and (3) as undeformed bladed kyanite crystals in quartz veins that are commonly folded. Kyanite and staurolite locally coexist, commonly sharing crystal faces in more iron-rich areas within or surrounding the quartz-kyanite pods. Locally, kyanite has replaced euhedral staurolite (Fig. 4d).

Zones of sericite schist (several m thick) enclose the quartz-kyanite pods, and grade outward to metarhyolite. A similar several-meter-wide layer connects the quartz-kyanite pods along strike. Altered albite porphyroclasts are common in the sericite schist layer, unlike the interiors of the quartz kyanite pods, where feldspars are rare or absent. Other minerals within the sericite layer include quartz, monazite, epidote, garnet, and Fe/Ti oxides. Asymmetric porphyroclasts in the sericite shells and quartz-kyanite pods may indicate more intense deformation than in the surrounding metarhyolite, where largely undeformed phenocrysts of feldspars and euhedral/embayed quartz are locally preserved (Simmons 1999).

Overlying the sericite schist layer are lenses of metarhyolite and a layer of pelitic schist (Fig. 3), composed of muscovite and quartz, with millimeter-scale porphyroblasts of biotite, chlorite and garnet, minor staurolite, magnetite and hematite. Overlying the pelitic schist and sandwiched between thin layers of metarhyolite, the Big Rock Conglomerate is a distinctive marker unit composed of stretched quartz, quartzite, and volcanic pebbles and cobbles, in a feldspathic, micaceous, and occasionally trough cross-bedded quartzite. The Big Rock Conglomerate comprises mostly well-rounded gravel-size cobbles, with occasional flattened wafer-like felsic clasts that may have originally been pumice.

Bedding is recognized as contacts between pebble-rich layers and pebble-free cross-bedded units; cross-bedding provides reliable younging directions that correspond with the overall stratigraphy of the area. Barker (1958) interpreted the Big Rock Conglomerate as a beach gravel deposit. Others have speculated the Big Rock Conglomerate represents a fluvial deposit, with associated sandstone and silt layers (University of New Mexico Field Camp mapping, 1992, 1996). Intense strain in this unit has obfuscated the original nature of the Big Rock Conglomerate, making it difficult to classify this layer as a volcaniclastic or volcanogenic sedimentary deposit.

Multiple layers of variable thicknesses of Vadito Group metarhyolite occur between the quartz-kyanite pods, the pelitic schist layer, and the Big Rock Conglomerate. Nearly euhedral, commonly undeformed microcline, albite and embayed quartz phenocrysts reside in a recrystallized, fine-grained matrix of quartz, K-feldspar, plagioclase, Fe/Ti oxides, rare biotite and very small garnet crystals. Several thin amphibolite, biotite and fluorite-rich veins occur within the metarhyolite near the quartz-kyanite pods.

Texturally heterogeneous, with interlayers of massive and more schistose layers, this unit is interpreted as a sequence of recrystallized rhyolitic flows, tuffs, and re-worked ash, similar to the Burned Mountain Metarhyolite of Barker (1958). The massive, quartz-feldspar phenocryst-rich Posos Lake metarhyolite overlies the Big Rock Conglomerate, and is also similar to the Burned Mountain Metarhyolite of Barker (1958). Feldspathic quartzite overlies this layer of metarhyolite, and becomes more quartz-rich up-section, towards the Ortega Quartzite. Several episodes of metamorphism and deformation completely recrystal-

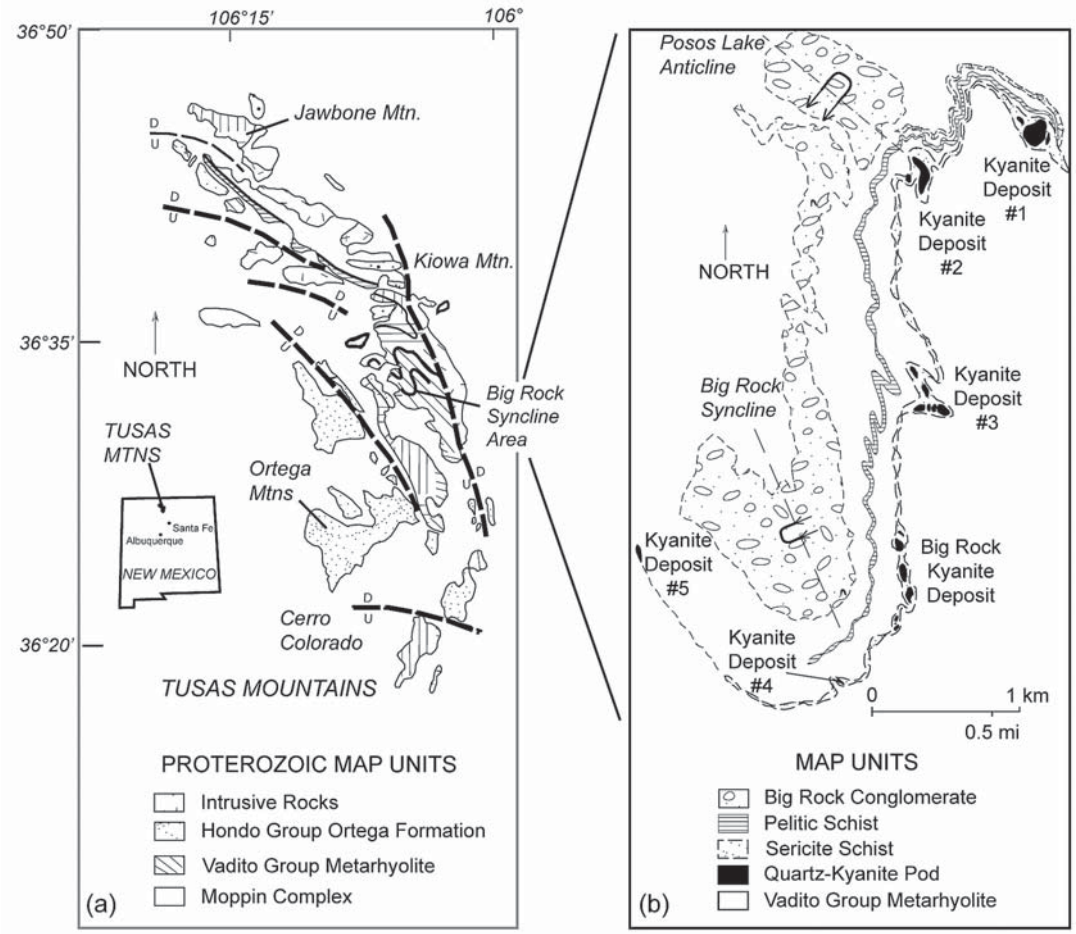

FIGURE 2. (a) Location of study area in Proterozoic rocks in northern New Mexico; (b) schematic geologic map of the study area.

lized the original porphyritic Vadito Group rhyolite into a fine-grained rock consisting of microcline, plagioclase and quartz, with biotite, sparse muscovite and epidote accessory minerals.

The distance between the Big Rock Conglomerate and the quartz-kyanite pod layer narrows between the southern pods (Big Rock Kyanite Deposit, Kyanite Deposits 4 and 5) and the northern Kyanite Deposits 1 and 2 (Fig. 2); this may be due to an early fault that tectonically thinned these layers, or may be related to original volcanic landforms and deposits, which are not always concordant.

GEOCHEMICAL METHODS AND RESULTS

Several lines of evidence point toward a hydrothermal/metasomatic origin to explain the unusual mineralogy of the quartz-kyanite pods: 1) high-Al bulk compositions, 2) the lack of alkali and alkaline earth elements, reflected by the scarcity of feldspars, and 3) the symmetrically zoned, discontinuous and lenticular nature of the quartz-kyanite pods. Geochemical studies were used to evaluate the nature of this metasomatism, and to distinguish primary (weathering and hydrothermal alteration) vs. secondary alteration in shear zones. Table 1 summarizes some of the physical and geochemical properties produced by these metasomatic processes.

Whole Rock Chemistry

Geochemical samples were collected from three traverses at short intervals through two of the quartz-kyanite pods and a zone of metarhyolite and sericite schist (Fig. 5). Samples were crushed in a Specs Industries ceramic Shatterbox and sieved through 100-mesh nylon screens. Major elements were analyzed using fused discs: 9 grams of $Li_2B_4O_7$ to 1 gram of sample fused at 1000º C. Trace elements were analyzed using pressed powders: 8.5 grams of sample to 1.5 grams boric acid pressed at 20,000 kg. Whole-rock compositional analysis was done on a Rigaku X-ray Fluorescence Spectrometer 3064M, with a rhodium target and an end window. All samples were analyzed against USGS and IWG International standards. Accuracy was tested by running random samples twice, and by running standards before, during, and after unknown analysis. Major element (wt %) and trace element (ppm) concentrations for each traverse are shown in Appendix 1.

The results of the whole rock study in Figure 6 show symmetrical depletion of K, Na, Ca, and total Fe from the metarhyolite host rocks towards the centers of Traverse 1 (Kyanite Deposit #1) and Traverse 3 (Big Rock Kyanite Deposit). Unlike Traverses 1 and 3, the geochemical profile across Traverse 2 (sericite schist

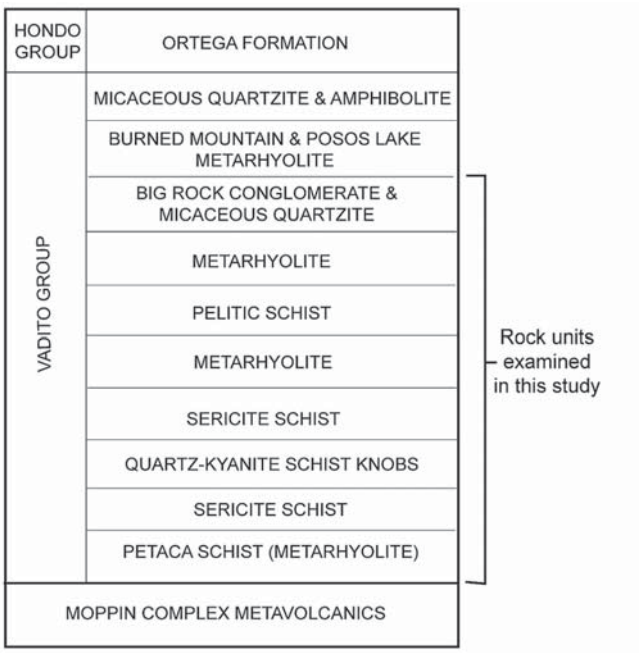

FIGURE 3. Stratigraphy of the Tusas Mountains (from Bauer & Williams, 1989; Lombardi, et al., 1996) and rock layers in this study.

layer) shows ambiguous patterns of element enrichment and depletion. The lack of similarity to the other traverses indicates the quartz-kyanite schist pods are discontinuous, and are thus unlike a soil horizon. The symmetrical nature of Traverses 1 and 3 through the quartz-kyanite pods, however, yield geochemical patterns that are consistent with both hydrothermal alteration and shear zone processes, but not of weathering profiles or paleosols (Table 1).

Isocon Analysis

Multiple alteration events may be indicated by the significant differences in bulk compositions, degree of mass transfer, and extent of volume change between the sampling traverses during metasomatism. The extent of mass transfer via element mobility, and subsequent volume gains/losses between altered and unaltered rocks from all three sampling traverses was evaluated using the isocon method of Grant (1986). The isocon method helps assess volume changes and concentrations of elements due to metasomatism (e.g. Selverstone et al., 1991; Newman and Mitra 1993; Grauptner et al., 2005; Warren et al., 2007).

Isocon diagrams help discern actual from relative element enrichments/depletions due to leaching of mobile cations (e.g. Ca, Na, Fe, K), by comparing these behaviors to immobile elements (e.g. Si, Al, Zr). Two or more elements of similar mobility that maintain a constant ratio between wallrock and altered rock during metasomatism are considered immobile and plot on a straight line (isocon) that passes through the origin (dashed lines in Figure 7). Other elements are compared to this reference line to determine enrichment or depletion: elements that plot above the immobile element isocon are enriched; those falling below the

TABLE 1. Physical and geochemical properties of paleosols, shear zones, and hydrothermal alteration zones compared to quartz-kyanite pods in this study.

PALEOSOL		SHEAR ZONE		HYDROTHERMAL ALTERATION		QUARTZ-KYANITE PODS	
laterally continuous		continuous		laterally discontinuous		laterally discontinuous	
stratiform		not stratiform		not stratiform		stratiform	
sharp upper contact		gradational upper contact		gradational upper contact		gradational upper contact	
gradational lower contact		gradational lower contact		gradational lower contact		gradational lower contact	
alteration reactions pre-deformation and pre-metamorphism		alteration reactions syn-deformation, pre- or syn-metamorphism		alteration reactions pre-deformation and pre-metamorphism		alteration reactions pre-shearing and pre- or syn-metamorphism	
symmetrical geochemical profile		symmetrical geochemical profile		symmetrical geochemical profile		symmetrical geochemical profile	
ELEMENT STABILITY ←→		↓ DEPLETION OR ENRICHMENT ↑					
↑↓←→	Al_2O_3	↑↓←→	Al_2O_3	↑↓←→	Al_2O_3	←→	Al_2O_3
↓	SiO_2	↑↓←→	SiO_2	↓↑	SiO_2	←→	SiO_2
↑↓	K_2O	↑↓	K_2O	↑↓	K_2O	↓	K_2O
↓	Na_2O	↓	Na_2O	↓	Na_2O	↓	Na_2O
↓	CaO	↓	CaO	↓	CaO	↓	CaO
↑	total Fe	↑↓	total Fe	↓	total Fe	↓	total Fe
↑↓	MgO	↑↓	MgO	↓	MgO	↓	MgO
?	MnO	?	MnO	?	MnO	↓	MnO
↑	TiO_2	↑↓	TiO_2	←→	TiO_2	←→	TiO_2

References: Gay & Grandstaff (1980); Grandstaff et al. (1986); Kimberley & Grandstaff (1986); Reimer (1986); Retallack (1986); Barrientos & Selverstone (1987); Golani (1989); Holland et al. (1989); Gall (1994); Krauskopf, K.B. & Bird, D.K., (1995); Anderson & Burnham (1983); Winchester (1984); Kerrick (1988); Grant (1986); Dipple et al. (1990); Dipple & Ferry (1991); Selverstone et al (1991); Newman & Mitra, (1993); VanBaalen (1993); Ague (1994); Ring, (1999); Meyer & Helmsley (1967); Burnham (1962); Beach (1976); Rose & Burt (1979); Hemley & Ellis (1983); Sillitow & Burnham (1984); Klein & Criss (1988); Criss & Champion (1991);Goff & Gardner (1994); Reimer(1986); Simmons (1999)

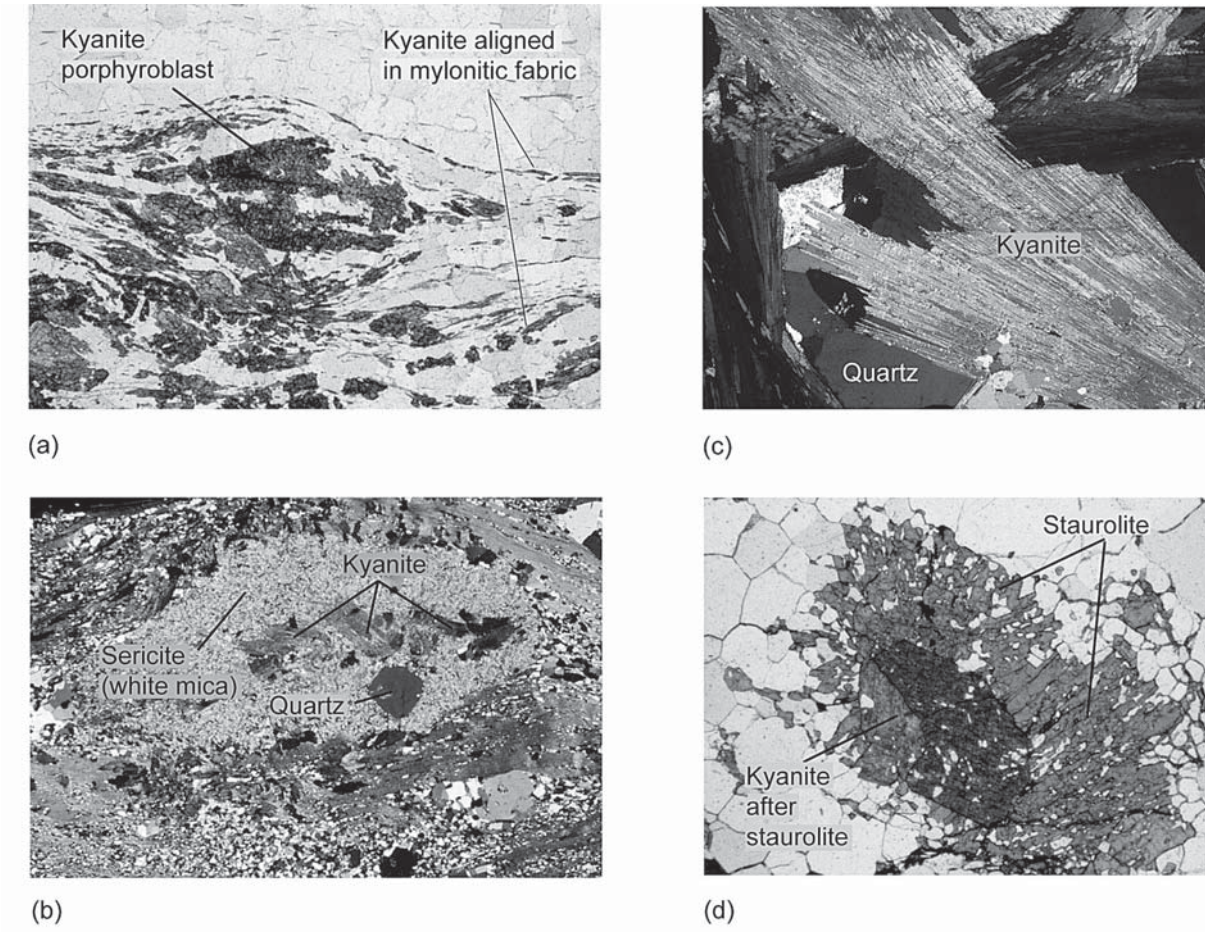

FIGURE 4. Photomicrographs of kyanite and staurolite; (a) kyanite porphyroblasts in mylonitic kyanite fabric (plane light); (b) sericite lump with kyanite crystallizing within (crossed polars); (c) Undeformed blades crystals of kyanite (crossed polars); (d) kyanite pseudomorph after staurolite (plane light).

isocon are depleted. If no alteration (no enrichment or depletion) occurs, elements plot on the immobile element isocon.

Whole-rock compositional data (Fig. 6) show that Al and Zr were neither greatly enriched nor depleted between the metarhyolite host rocks at the edges of the traverses, and the zone of quartz/kyanite/sericite. Al and Zr were therefore chosen as the immobile elements that define the mass transfer isocon. The slope of the immobile element isocon, relative to the constant (1:1) mass isocon (solid lines in Figure 7), gives an estimate of the volume gains/losses that accompanied alteration. If the immobile element isocon is located above the constant mass isocon (i.e. has a steeper negative slope), volume was lost; if it falls below the constant mass isocon, volume was gained. Small deviations between the isocons represent small volume changes, and vice versa.

The isocon diagrams in Figure 7 compare element enrichment/depletion in the traverse samples to an average metarhyolite composition of the Vadito Group in the Tusas Mountains (Table 2), normalized to 100%. The diagrams show that Ca, Na, Fe, K and Mg are generally depleted across Traverse 1 and 3, which are near mirror images of each other, possibly indicating multiple alteration processes, or local differences in fluid:rock compositions. Traverse 2 isocons show mass transfer toward the sericite schist layer, but ambiguous element enrichment/depletion patterns. Rock layers across Traverse 2 are poorly exposed, and may include several interfingering layers of altered and non-altered metarhyolite, yielding ambiguous geochemical patterns.

EVALUATION OF QUARTZ-KYANITE GEOCHEMISTRY AND HYDROTHERMAL ALTERATION

Symmetrical chemical profiles, scarcity of feldspars, and variations in mineral assemblages across the quartz-kyanite pods, including white mica and altered albite in the sericite schist layer are indicators of hydrothermal alteration. At shallow depths in the crust, circulating fluids of moderate to high temperature and low to neutral pH commonly produce concentric zones of altered mineral assemblages, as the host rock is converted to new sets of minerals more compatible with the fluid composition. Table 3 summarizes some of the properties and minerals associated with hydrothermal alteration zones.

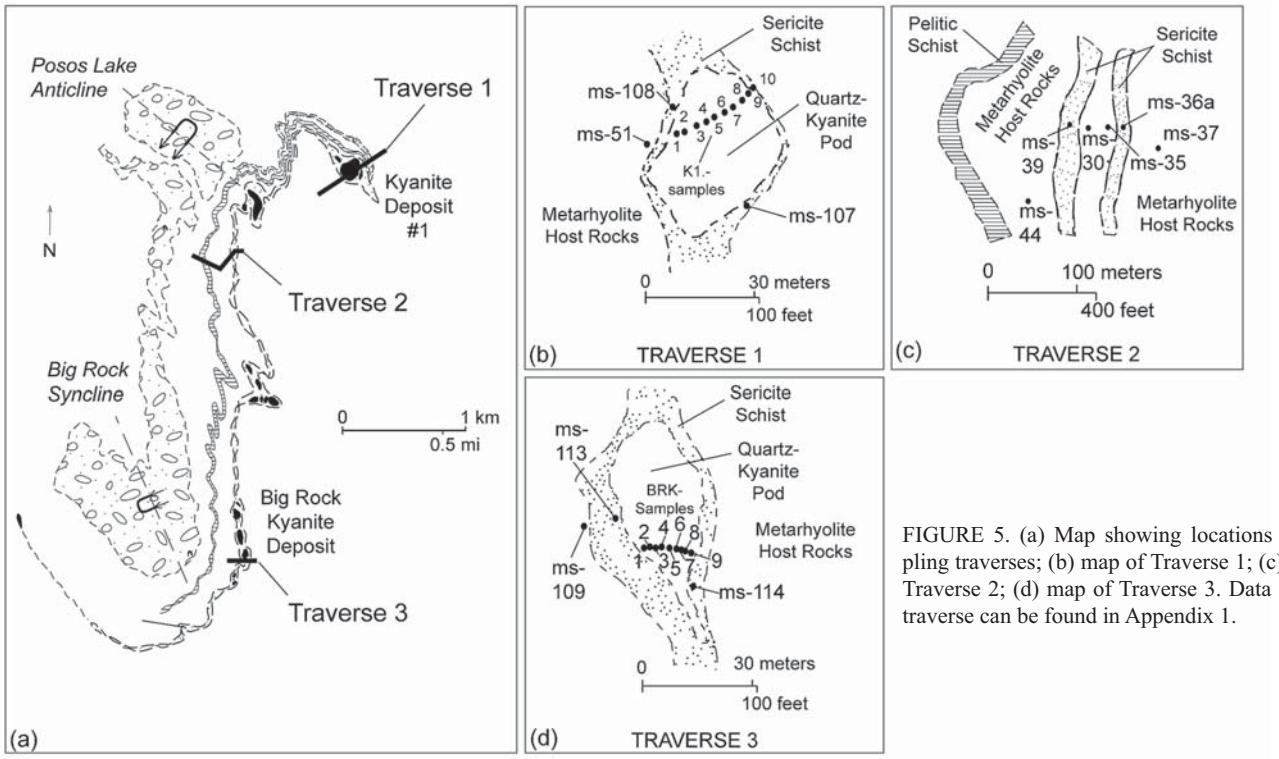

FIGURE 5. (a) Map showing locations of sampling traverses; (b) map of Traverse 1; (c) map of Traverse 2; (d) map of Traverse 3. Data for each traverse can be found in Appendix 1.

Zones of most intense alteration are adjacent to the conduit carrying hot hydrothermal fluids (Meyer and Hemley, 1967; Piranjo, 2010), that can reach temperatures of ~700ºC (Fig. 8a). Al is enriched as the incoming fluid leaches Ca, Na, Mg, Fe, and K from minerals in the host rock (Bronson et al., 1952; Piranjo, 2010). Alteration proceeds outward, toward unaltered wallrock, from advanced argillic through sericitic (also known as phyllic alteration), argillic, and finally, propylitic (Fig. 8b).

The complete decomposition of feldspars in the innermost advanced argillic zone produces the mineral assemblage: kaolinite group minerals + quartz + hematite + limonite. At higher temperatures, given high silica fluids, advanced argillic alteration can produce pyrophyllite, K-feldspar + biotite, or K-feldspar + chlorite + magnetite (Wohletz and Heiken 1992; Pirajno, 2010).

Sericitic alteration produces sericite + quartz, also by the decomposition of feldspars, and commonly occurs in fault structures or zones in hydrothermal systems (e.g. Wohletz and Heiken, 1992, Brown et al, 2006). Decomposition of feldspars continues through the argillic alteration zone, producing more kaolinite group minerals including dickite and halloysite, and illite-type

TABLE 2. Whole-rock major-element chemistry of Vadito Group metarhyolite samples.

	BMR	ms-35	ms-37	ms-38	ms-30	ms-51	ms-109	ms-66	AVERAGE
SiO_2	75.87	77.87	77.42	75.67	76.88	76.45	77.77	74.50	76.55
Al_2O_3	11.48	12.25	11.87	13.81	13.56	13.61	12.08	13.26	12.74
P_2O_3	0.05	0.04	0.05	0.03	0.06	0.04	0.04	0.05	0.05
CaO	0.55	0.42	0.42	0.51	0.52	0.32	0.39	0.43	0.45
TiO_2	0.40	0.09	0.11	0.11	0.10	0.13	0.11	0.21	0.16
$FeO+Fe_2O_3$	2.58	1.27	1.57	1.57	1.43	1.98	1.79	2.65	1.86
Na_2O	3.31	2.57	3.56	3.84	2.59	3.00	3.06	2.39	3.04
K_2O	4.93	4.48	4.71	2.39	3.91	4.26	5.12	6.23	4.50
MgO	0.30	0.16	-	0.08	0.02	0.18	0.29	0.28	0.16
MnO	0.07	0.03	0.01	0.10	0.03	0.02	0.01	-	0.03
TOTAL	100.00	100.00	100.00	100.00	100.00	100.00	100.00	100.00	100.00

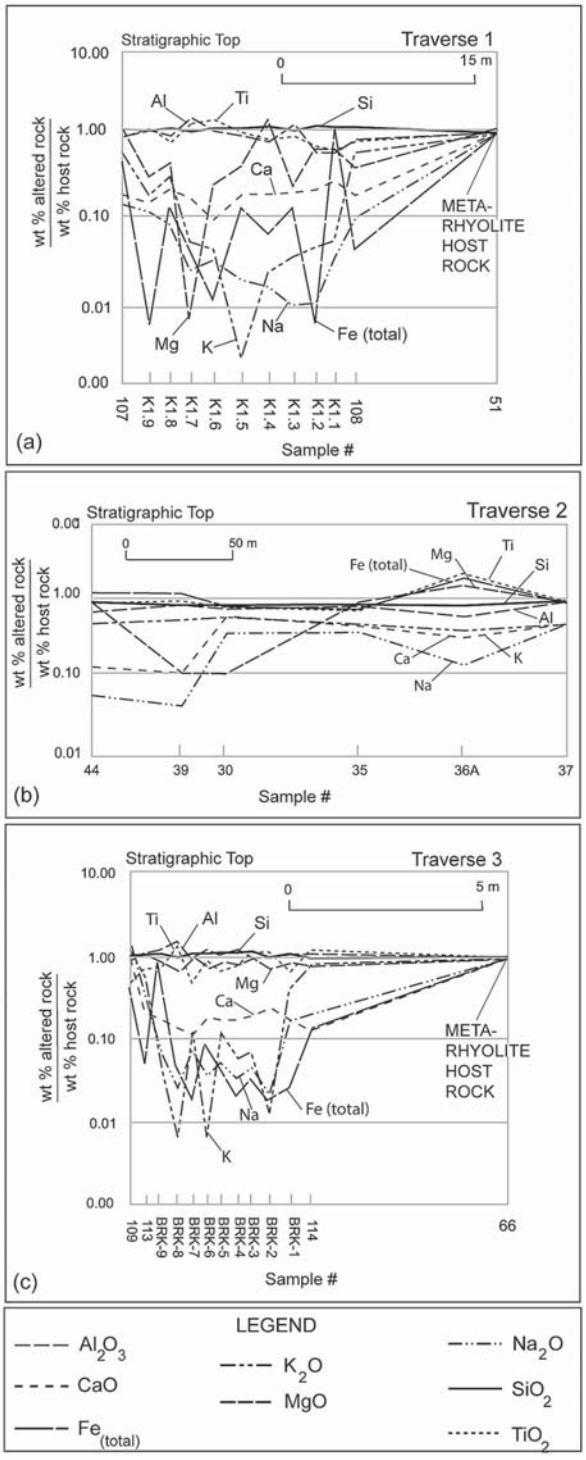

FIGURE 6. Geochemical profiles showing element enrichment/depletion across the sampling traverses. (a) Traverse 1 shows strong symmetrical depletion of Ca, Na, K, Fe, Mg toward the center of the quartz-kyanite pod; (b) Traverse 2 shows symmetrical enrichment of Fe, Mg, Ti and depletions of Ca, Na, K through the eastern sericite schist layer, but ambiguous patterns throughout the rest of the traverse; (c) Traverse 3 shows strong symmetrical depletion of Ca, Na, K, Fe toward the center of the quartz-kyanite pod.

TABLE 3. Properties of hydrothermal alteration zones.

Advanced Argillic	Sericitic	Argillic	Propylitic
Higher T, low pH	Lower T, low pH	Lower T, low pH	Lower T, neutral pH
Decomposition of feldspars	Decomposition of feldspars	Decomposition of feldspars	Decomposition of Fe,Mg-bearing minerals (e.g. biotite, amphibole, pyroxene)
Kaolinite, quartz, hematite, limonite, pyrophyllite (high T)	White mica, quartz	Clay minerals: kaolinite, illite, smectite	Quartz, chlorite, epidote, albite, adularia, actinolite, carbonate

phyllosilicates such as sericite and other clay micas. Argillic alteration is a low pH process that also produces a wide variety of clay minerals, including kaolinite, illite and smectite.

Propylitic alteration occurs in the outermost zones, furthest from the hydrothermal fluid conduit, under neutral pH conditions and lower temperatures. High Fe and Mg minerals, such as chlorite, actinolite and epidote form from the decomposition of biotite, amphibole or pyroxene, giving propylitically altered rocks a green tint.

The hypothetical alteration zones in Figure 8b shows the relationships between the different styles of alteration discussed previously, and compares well with the schematic map of the mineral zones in the middle knob of the Big Rock Kyanite deposit (Fig. 8c). Mining in the 1920's exposed a large zone of apparent kyanite pseudomorphs after pyrophyllite within the interior of this quartz-kyanite pod (Fig. 9), perhaps indicating a zone of advanced argillic alteration. The scarcity of feldspars and the presence of paragonite in the quartz-kyanite pods may also indicate albitic alteration common to some hydrothermal systems, where Na-plagioclase alters to paragonite (Gammell, 2007).

The 'staurolite-quartzite bands' of Shreyer and Chinner (1966) that crop out beneath piles of tree and rock debris at the base of the western slope of the Big Rock Kyanite Deposit in Figure 8b may be a zone of metamorphosed propylitically-altered rhyolite. Concordant with the fabric in the quartz-kyanite pods and sericite schist, these layers of staurolite + chlorite + garnet + quartz are in sharp contact with the sericite schist, with a grain-size coarsening away from the contact. Schreyer and Chinner (1966) attempted to characterize the staurolite layers first as igneous intrusions, then later as metasediments, but neither the chemical nor the mineralogical composition of the layer resemble any known igneous or sedimentary rock. A propylitic alteration zone, however, can explain this unusual layer where Mg and Fe are concentrated. (Afshooni et al. 2011; Norman, et al. 1991; Piranjo 2010).

The quartz-kyanite pods, sericite schist, pelitic schist and Big Rock Conglomerate may be components of a fossil hydrothermal system along a fracture zone in a small caldera or other volcanic landform in which hydrothermal fluids were channeled (Fig. 10). The Big Rock Conglomerate sandwiched within the Vadito Group metarhyolite is likely a volcaniclastic unit, and may be

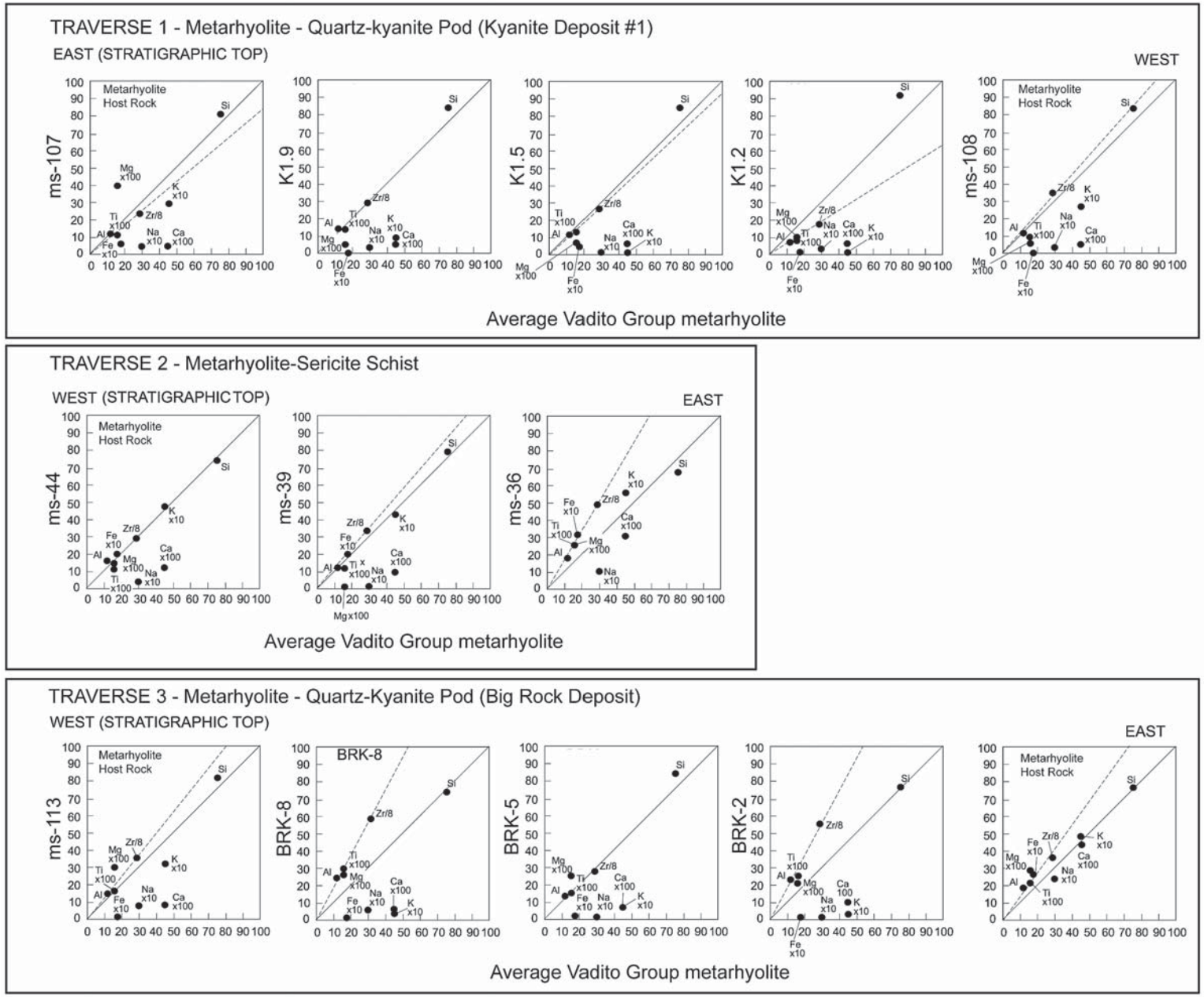

FIGURE 7. Isocon diagrams comparing the average metarhyolite composition from Table 3 (x-axes) to the compositions of the samples from the sampling traverses (y-axes). Solid lines represent the constant mass isocon; dashed lines represent the immobile element isocon. Elements plotting above dashed lines are enriched; below the dashed line, elements are depleted. Volume gains are indicated where the dashed line is below the solid line, losses where the dashed line is above the solid line.

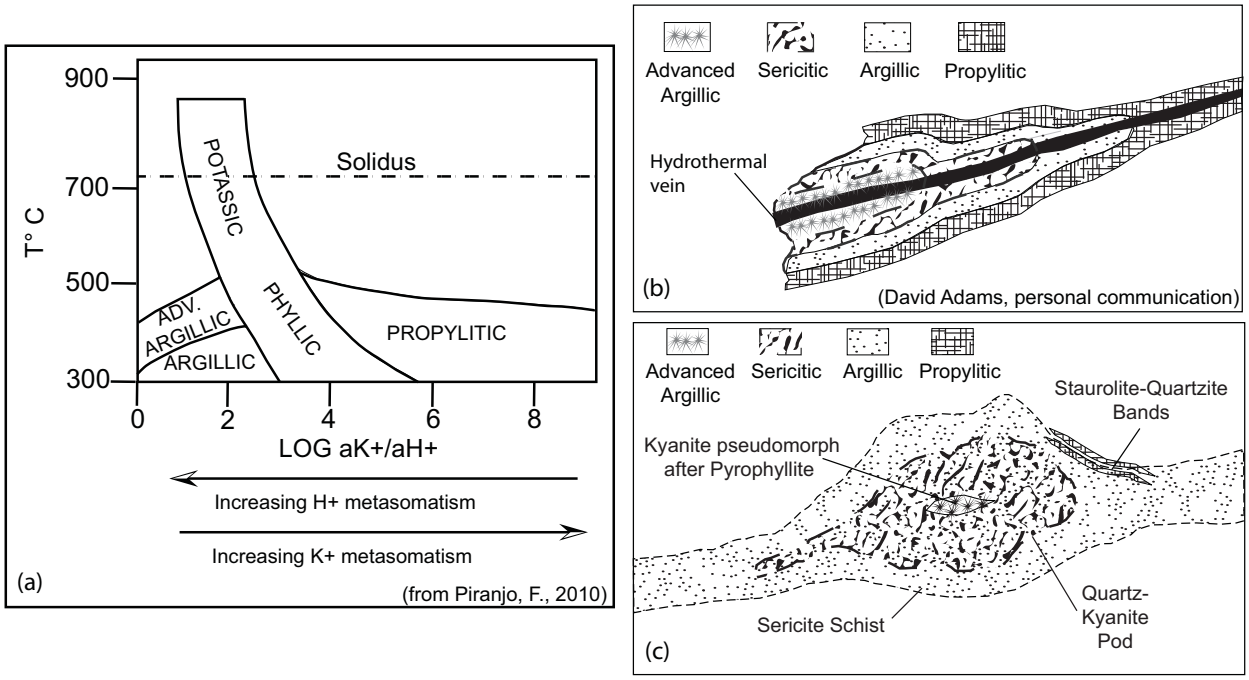

FIGURE 8. (a) Temperature vs. alteration fields in hydrothermal alteration systems; (b) schematic map of a hypothetical hydrothermal system, showing layers of alteration according to intensity and proximity to vein system; (c) schematic geologic map of the Big Rock Kyanite Deposit relating zones of alteration to the hypothetical model in (b).

the remnants of a tuff ring within a small caldera system, and the quartz-kyanite pods originated from hydrothermal alteration along ring fractures. Alternately, vents or fumaroles through the conglomeratic and rhyolitic layers may have produced the compositions and distribution of the quartz-kyanite pods.

Bulk composition and mineral assemblages produced by hydrothermal alteration (clay minerals, sericite, magnetite, and hematite) are compatible not only with the quartz-kyanite and sericite schist, but the host rhyolite rocks as well. Alteration in the quartz-kyanite pods, sericite and pelitic schist layers is localized, as is typical of hydrothermal deposits, and unlike the extensive regional alteration that might occur due to a contact metamorphism from a nearby igneous intrusion. Ubiquitous swarms of quartz veins of varied thickness within all of the quartz-kyanite pods, as well as in the adjacent metarhyolite, would also be consistent with a hydrothermal system operating during or after Vadito Group volcanism.

The mineralogy and geochemistry of the quartz-kyanite pods and the sericite-rich layer are different, yet both can be argued to be alteration products of the Vadito Group rhyolite. All of the clay minerals produced in hydrothermally altered rhyolites are of the kaolinite and illite group (Bundy 1958; Hurst and Kunkle 1985; Mao and Bierlein 2005), providing the appropriate composition to produce kyanite, or one of its polymorphs, depending on metamorphic temperature and pressure.

The lack of similarity between volume gains and losses and element enrichment/depletion patterns between the three sampling traverses suggests more than one alteration process. Kyanite pseudomorphs after staurolite (e.g. Fig. 4d) may indicate mobilization of Fe during metamorphism. Our favored hypothesis is that early hydrothermal alteration associated with Vadito Group volcanism produced the original Al-rich bulk compositions of the quartz-kyanite pods and sericite schist layer, and provided a weak zone along which later D_1 fluids associated with shearing during metamorphism further altered these rocks and maintained the link between them.

DEFORMATION AND METAMORPHISM

Four deformational events are observable at macroscopic, mesoscopic and microscopic scales (e.g., Williams 1990; 1991; Williams et al., 1999). Following standard conventions, our nomenclature is to use F_1, S_1, and L_1 for the folds, foliations and surfaces, and lineations (respectively) that were produced during the first deformation (D_1). These are identified as the oldest tectonic structures because they are locally refolded or overprinted (Hobbs et al., 1976) by second-generation structures F_2, S_2, L_2, produced during the most intense deformation event D_2. The dominant regional foliation, S_2, is also deformed locally by F_3, S_3, L_3, developed during a D_3 shortening event. Low strain events during D_4 produced kinks and discontinuous foliations that we designate F_4, S_4, and L_4. The styles and inferred timing of each event are depicted in Figure 11.

The first event (D_1) is represented by a bedding-parallel foliation (S_1) that is marked by aligned kyanite and muscovite in the quartz-kyanite pods, and foliation in the pelitic schist and metarhyolite, both of which are folded (with bedding) in the hinges of F_2 folds. Though fairly rare and not observed at map scale,

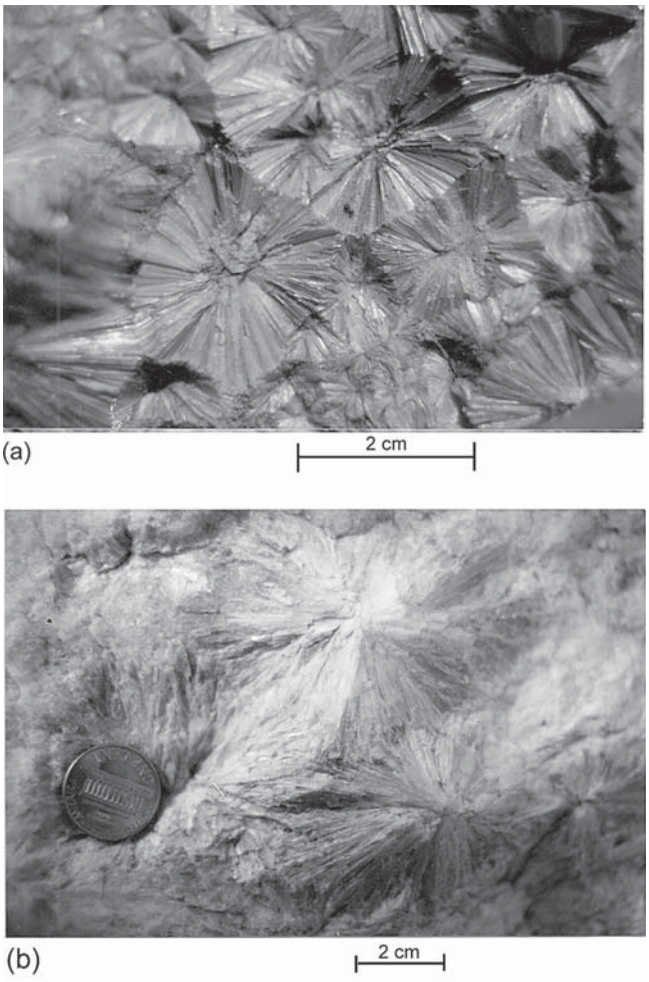

FIGURE 9. Photographs of (a) pyrophyllite rock from the Hillsborough Mining District, Carolina Slate Belt, NC; (b) kyanite pseudomorph after pyrophyllite from Big Rock Kyanite Deposit.

F_1 folds were initially sub-recumbent isoclinal folds that occur at outcrop and thin section scales (Fig. 11a). Map scale stratigraphic pinch-outs along S_1 in the quartz-kyanite/sericitic layer are discontinuities that may be related to thrusting (Williams et al., 1999), such that map scale expressions of D_1 are likely to involve thrust ramps and shear zones that were modified during later deformations and hence are difficult to recognize.

Lineations plunge shallowly NE-SW, even though S_1 planes have been reoriented by F_2 folding. D_1 microstructures involving kyanite fabrics have been strongly overprinted by D_2 foliation and are commonly characterized by a composite fabric. Top-to-the south shear sense is documented along a possible S_1 shear zone in several of the kyanite knobs. This is in contrast to the overall NW- directed vergence inferred from F_2 fold asymmetry and previous models for NW- directed transport during D_2 fold-thrust progression (Williams, 1991). Other studies of similar age rocks elsewhere in northern New Mexico Proterozoic rocks indicate top-to-south shearing mainly in younger fabrics (Grambling et al., 1989; Pedrick, 1995).

D_2 was the result of NE-SW shortening and resulted in the formation of the large-scale NW-trending F_2 anticlines and synclines of the Tusas Mountains. Figure 11b shows the effects of a progressive NE-SW (north-verging) shortening episode (D_2) that produced the most penetrative fabric (S_2), a northwest-trending and steeply SW-dipping foliation that is axial planar to map scale F_2 folds. Pebbles in the Big Rock Conglomerate tend to be flattened and elongated (L>S) and are aligned in the F_2 axial plane fabric with elongation lineation plunging 50 to 220 (Williams, 1991).

D_3 produced north-south trending axial planar cleavages (S_3) in folded Big Rock Conglomerate pebbles, recording east-west (D_3) shortening in map-scale F_3 folds, which refold the earlier, larger F_2 folds (Fig. 11c). Mushroom-style interference patterns have been mapped in the Big Rock Conglomerate (University of New Mexico Field Camp mapping 1992, 1996).

The fourth deformational episode, D_4, is represented by a weak NW to E-W-trending fabric (S_4), visible as a minor crenulation cleavage of S_3 in the more micaceous layers (Fig. 11d). At map scale, F_4 may be expressed as a slight re-orientation of minor F_2 folds. Unoriented, undeformed bladed kyanite crystals in thin sections, and hand samples of large (~5cm) kyanite pseudomorphs after pyrophyllite suggest late (syn/post-S_4) crystallization.

Thin sections from the quartz-kyanite pods show quartz inclusion trails within staurolite and kyanite pseudomorphs after staurolite (pre-S_1?) that are aligned in S_1/S_2 (Fig. 12a). Aggregates of semi-radial kyanite crystals within paragonite (or other white mica) aligned in S_1, surrounded by anastomosing, grain-sized reduced zones of kyanite + white mica (Fig. 12b, c, d, e, f), suggest kyanite existed prior to and during S_1 shearing. Knobby lumps (~2-3 cm) in the Big Rock Kyanite outcrop suggest the former presence of andalusite porphyroblasts, but in thin section, these are chunks of radial-habit kyanite, partially crystallized from white mica. Not uncommonly, andalusite can replace earlier forming pyrophyllite or chloritoid in hydrothermal zones (Morton et al., 1996; Deere et al., 1997; Schmidt et al., 2006), preserving the radial habit common to both. Chloritoid occurs infrequently within the quartz-kyanite pods, as small aggregates strung out within S_1.

D_2 minerals include chloritoid as an axial planar mineral to F_2 folds (Fig. 13a). Biotite overgrew S_2, shown by alignment of inclusion trails (Fig. 13b). Garnet overgrew S_2 prior to initiation of S_3 deformation (Fig. 13c). Chlorite and staurolite overprinted S_2, and may have been rotated by S_3, as shown by deflected inclusion trails (Fig. 13d, e). Syn-S_2 staurolite overgrew and displaced Q-M domains, the typical S_2 fabric (Fig. 13f). Syn-S_2 chlorite, staurolite and chloritoid within the staurolite bands at the base of the northernmost Big Rock Kyanite deposit are pre- and syn-S_2 minerals, that are axial planar to map-scale F_2 and 10-meter-scale F_3 folds. Each of these minerals can also form in hydrothermal zones (Bonnett and Corriveau 2007; Deere ,et al., 1997) and may have been a constituent of this layer prior to deformation.

Biotite (Fig. 14a) and chlorite (Fig. 14b) overgrew S_2 prior to and during the onset of crenulations associated with S_3/S_4 fabrics, as shown by truncation of Fe/Ti oxides inclusion trails, the alignment of the biotite and chlorite porphyroblasts in the axial

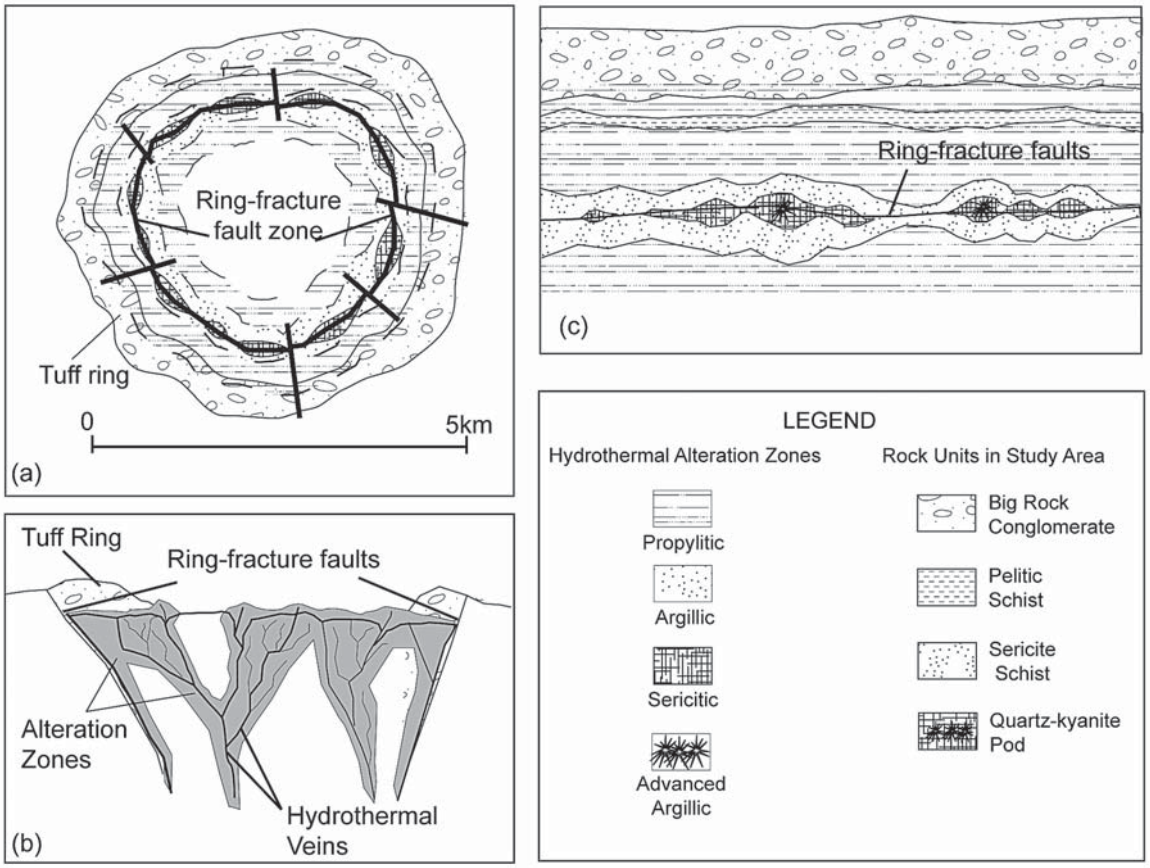

FIGURE 10. Schematic diagrams of proposed model of hydrothermal system along the quartz-kyanite layer during Vadito volcanism; (a) map of proposed ring fracture and hydrothermal alteration zones; (b) cross section of small caldera/ring fracture zone; (c) enlarged map view of proposed ring fracture faults relative to surrounding rock layers; and zones of alteration.

plane of F_4, and by the truncation of the outside fabric against the biotite. These lines of evidence, and the folded "tails" in post-S_2 chlorite (Fig. 14c), suggest chlorite growth during D_4/S_4. Monazite and zircon inclusion trails in biotite and chlorite porphyroblasts may be defining earlier (S_1 and/or S_2) fabrics (Fig. 14c).

PRESSURE-TEMPERATURE-DEFORMATION HISTORY

Quartz-kyanite oxygen-isotope thermometry on two distinct varieties of kyanite from the Big Rock Kyanite Deposit produced $\delta^{18}O$ values of 7.0 and 7.5 per mil, corresponding to inferred temperatures of formation of 530ºC and 590ºC, respectively (Simmons and Larson, 2001). Quartz-kyanite thermometry reports temperatures of growth, which are not necessarily peak metamorphic temperatures (Larson, 2003). There is no evidence, however, that metamorphic temperatures exceeded 590ºC and the $\delta^{18}O$ temperatures correlate with nearby areas in the Tusas Mountains (e.g. Williams, 1991). The different temperature estimates indicate two generations of kyanite growth, assuming the quartz $\delta^{18}O$ value did not change during the two growth periods.

Syn-S_1 minerals except for kyanite can all be related to formation under hydrothermal alteration conditions (described in a previous section), where temperatures may have approached 600ºC at shallow sub-surface depths (1-2 km). Under greenschist facies conditions, kyanite and chloritoid can occur together in high Al-rocks, an assemblage that is usually recognized as an indicator of higher-grade metamorphism (Deere et al., 1997). In hydrothermal systems, where fluids are commonly acidic, the lower stability limits of both andalusite and pyrophyllite are significantly depressed to conditions at which andalusite would have not otherwise been stable (Deere et al., 1997).

Thus, we consider the possibility that early high temperatures may reflect localized hydrothermal alteration. However, these temperatures are also compatible with conditions of prograde and peak metamorphism during D_2 deformation reported in Williams (1990; 1991) and Williams et al. (1999).

The proposed P-T path (Fig. 15) begins at near-surface depths during hydrothermal alteration of Vadito Group rhyolite, with the production of kaolinite (<300ºC), followed by pyrophyllite, a mineral commonly produced in hydrothermal alteration zones (Sykes and Moody, 1978); Brown et al., 2006) at temperatures around 325ºC. The S_1/S_2 assemblage in the quartz-kyanite

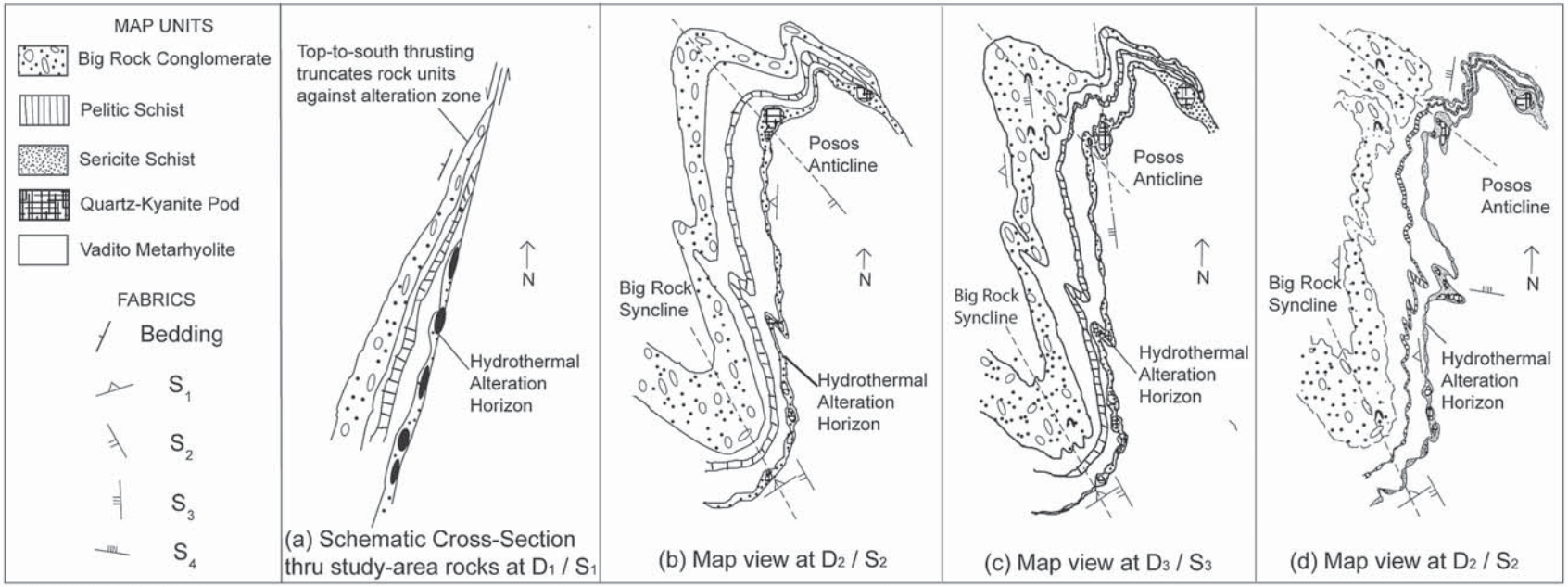

DEFORMATION (D)	1	2	3	4
FOLD GENERATION (F)	RECUMBENT FOLDS (?) & BEDDING-PARALLEL THRUSTS	MAP-SCALE TIGHT RECLINED FOLDS NE-VERGING, NW PLUNGING	UP TO 10 METER-SCALE FOLDS	SMALL-SCALE OPEN UPRIGHT FOLDS & CRENULATIONS
FOLIATION (S)	BEDDING-PARALLEL INITIALLY SUB-HORIZONTAL	AXIAL PLANE TO F_2 FOLDS NW-TRENDING STEEPLY SW-DIPPING MAIN SHORTENING FABRIC FLATTENED BRC PEBBLES	N-TRENDING SUB-VERTICAL AXIAL PLANE TO F_3 FOLDS & FOLDED BRC PEBBLES	VARIABLE, BUT GENERALLY E-W-TRENDING CRENULATON OF S_1 TO S_3 DIP IS SUB-VERTICAL?
METAMORPHIC MINERALS	PRE(?)-SYNS$_1$ SYN-S$_1$	SYN-S$_2$ / S$_3$		SYN-S$_4$
	Q-K PODS:	Q-K PODS: STAUROLITE BANDS: PELITIC SCHIST:		STAUROLITE BANDS: Q-K PODS: PELITIC SCHIST:
	PYROPHYLLITE ANDALUSITE CHLORITOID PARAGONITE / KYANITE STAUROLITE	KYANITE STAUROLITE CHLORITOID / STAUROLITE BIOTITE CLORITE / GARNET BIOTITE CLORITE		BIOTITE CLORITE / KYANITE / BIOTITE CLORITE
SHEAR SENSE	TOP-TO-SOUTH	TOP-TO-NORTHEAST		
TIMING (Ga)	POST-1.65	1.65-1.42	Ca.1.42	Ca.1.42

FIGURE 11. Relationships between deformation, fabrics, folds, metamorphic minerals and time.

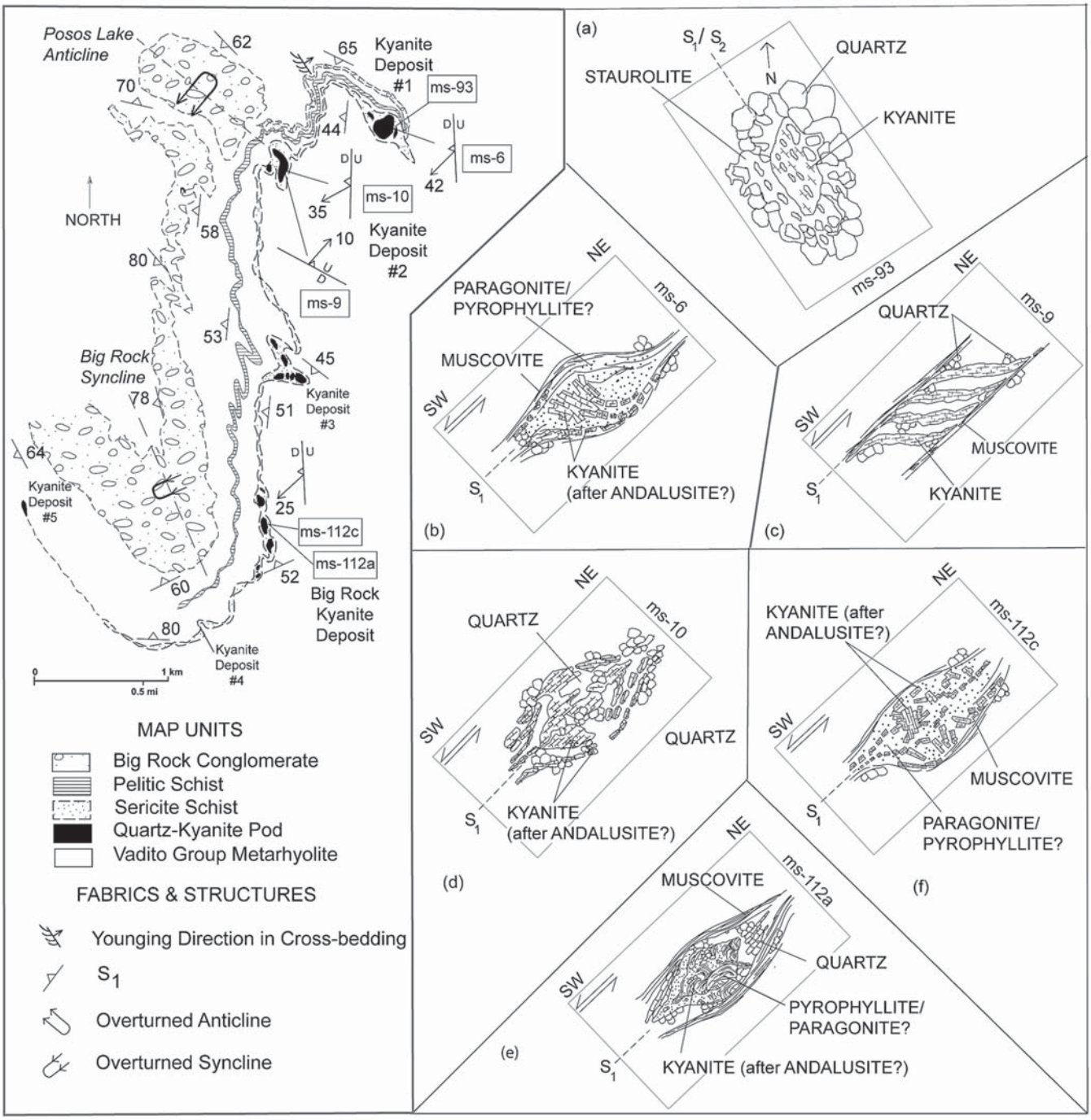

FIGURE 12. Metamorphic minerals and S_1/S_2 fabrics; (a) is a map-view thin section; b,c,d,e are cross-sectional views (thin sections cut perpendicular to foliation and parallel to lineation).

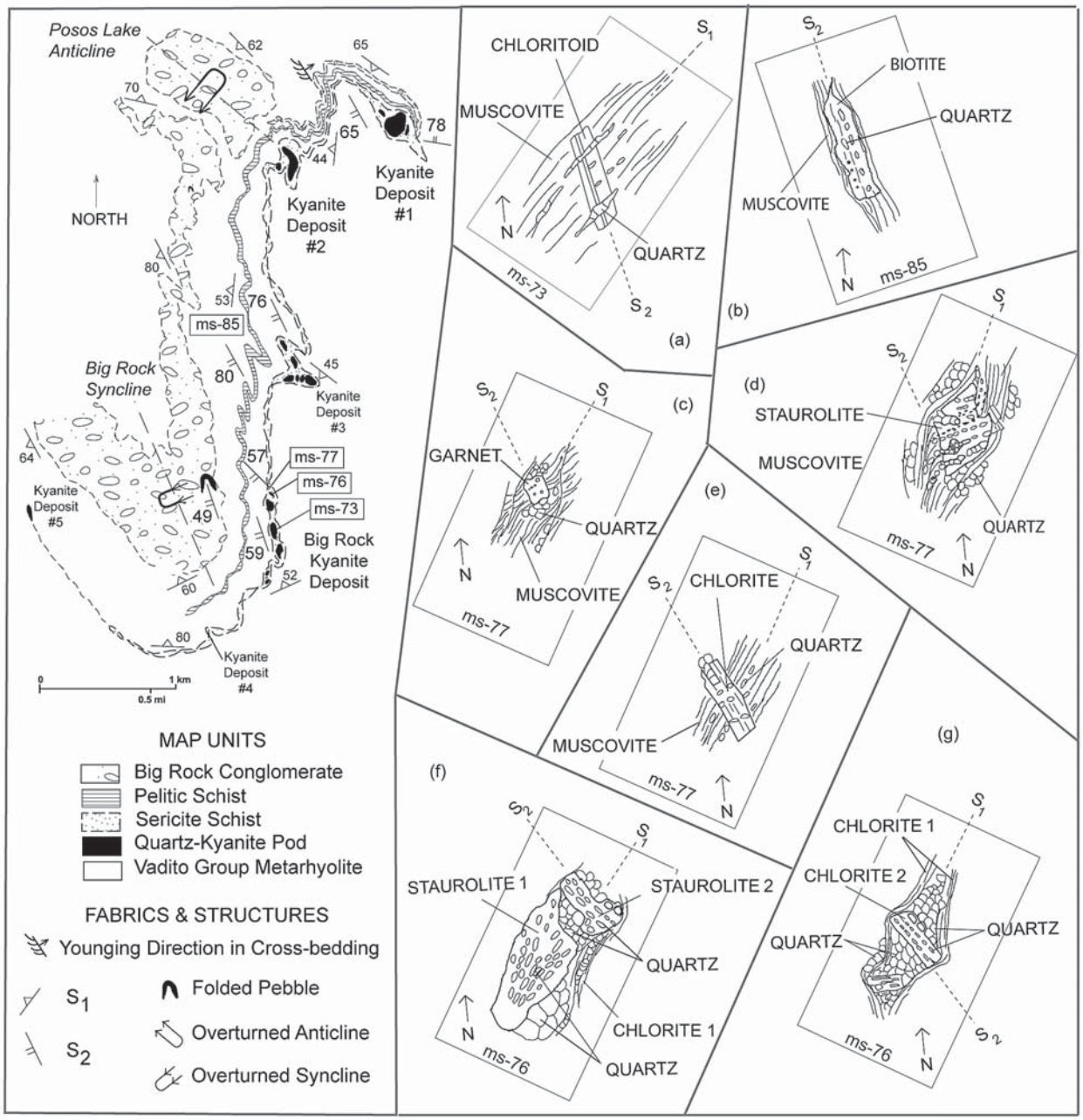

FIGURE 13. Metamorphic minerals associated with S_2 deformational fabrics, in map-view thin sections.

pods:,ky + staur + ctd + bt, indicates maximum P-T conditions of around 490ºC, and are correlated to the regional pressure (~400 MPa) in other areas of the Tusas (e.g. Williams, 1991, 1999) during development of S_2.

Progressive deformation buried these rocks to sufficient pressure for kyanite to crystallize within the quartz-kyanite pods, commonly as pseudomorphs after lower grade hydrothermal minerals. Oxygen-isotope data indicate a thermal peak of ~590ºC, which may refer to the peak temperature achieved during hydrothermal alteration, but is more likely is related to metamorphism. According to mineral assemblages (Figs. 12, 13, 14), the peak pressure of 400 MPa occurred at ~500ºC, during D_2 deformation and metamorphism.

CONCLUSIONS

Summarizing available data from this study and from previous studies, the following relative timing sequence is hypothesized:

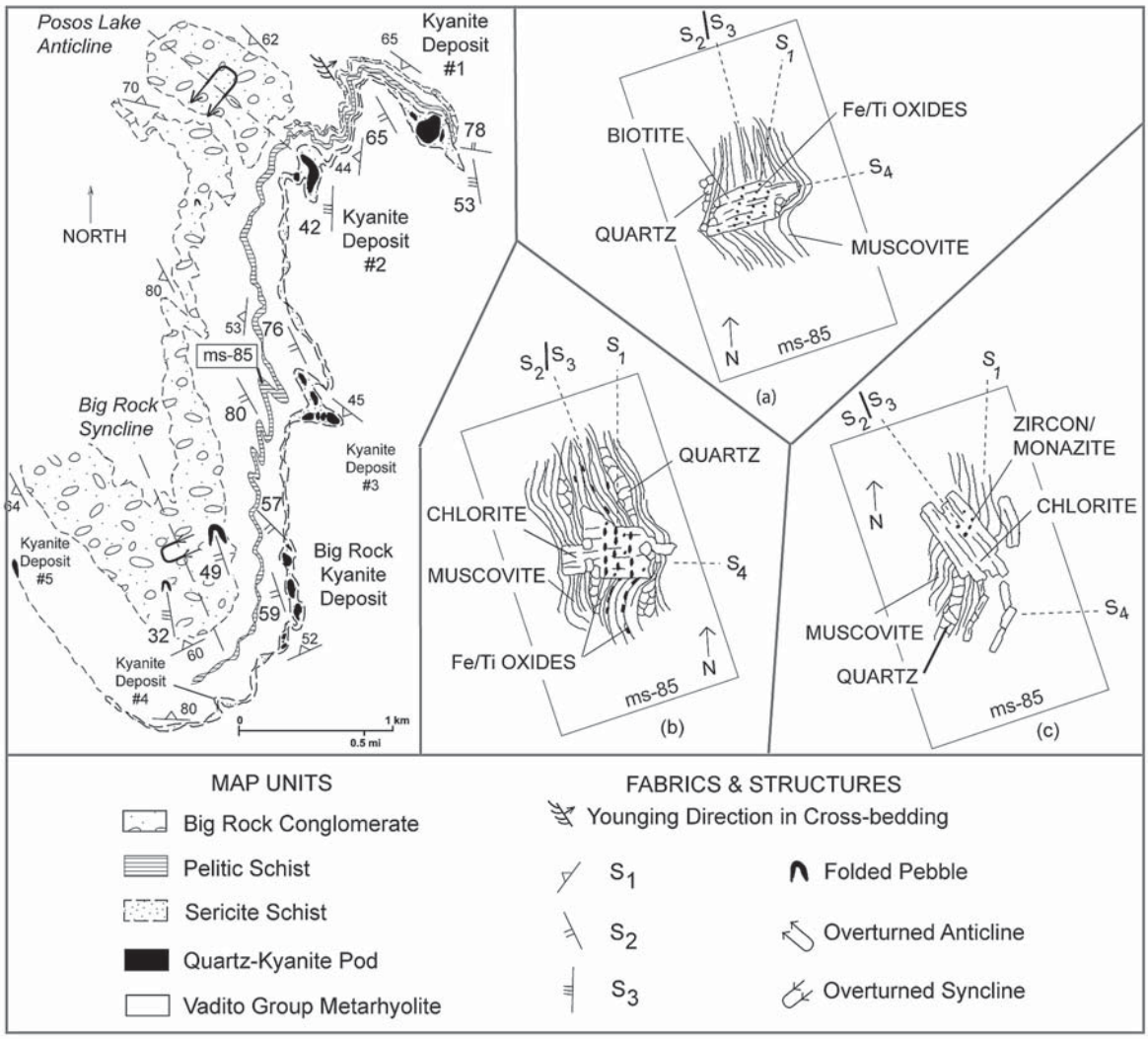

FIGURE 14. Metamorphic minerals associated with S_3/S_4 and overprinting relationships to S_1/S_2 fabrics, in map view thin sections.

1 - An argillic hydrothermal alteration system may have been active during Vadito Group volcanism, based on geochemistry, mineral compositions, textures, mineral zonation in the quartz-kyanite pods and sericite schist shells.

2 - Kaolinite-group clay minerals were likely produced by hydrothermal alteration of rhyolite, and may have been followed by a pre-S_1 assemblage that could have included pyrophyllite, andalusite, chloritoid, staurolite and biotite by caused by high temperature related to advanced argillic hydrothermal alteration, contemporaneous with 1.7 Ga Vadito Group volcanism.

3 - Early top-to-south movement along S_1 in the quartz-kyanite pods is likely due to fabric reactivation during F_2 folding. Movement may also have occurred along an early hydrothermal fault system at temperatures that may have approached 590ºC and produced pre-S_1 asymmetric porphyroblasts of low-pressure aluminosilicates (e.g. andausite, pyrophyllite, chloritoid).

4 - Kyanite replaced pyrophyllite, and may also have replaced andalusite in the asymmetric porphyroblasts, during D_1 deformation and metamorphism that aligned the quartz-kyanite pods in S_1.

5 - Peak metamorphic conditions were achieved during D_2 at a temperature of ~500ºC, and regional pressure of ~400 MPa. North verging shortening produced S_2 fabrics that are post-1.65 and pre-1.4 Ga. Kyanite crystallization continued through D_4, developing large undeformed crystals.

6 - Kinking and small folds in quartz-kyanite rocks and weak crenulations of variable orientation were produced by S_4, probably syn-1.4 Ga.

ACKNOWLEDGMENTS

We thank reviewers Christopher Andronicos and Peter Davis, whose thoughtful and helpful comments improved this paper. We are grateful for the funding from the Geological Society of Amer-

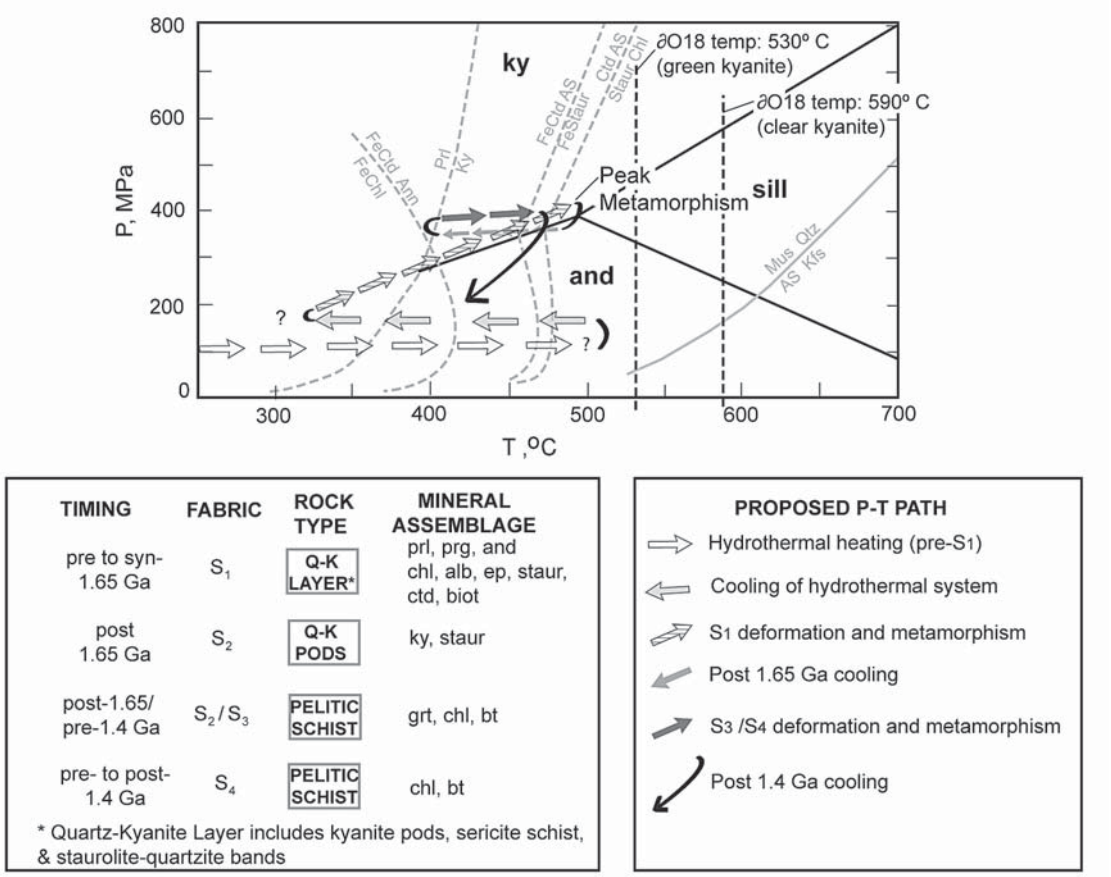

FIGURE 15. Proposed pressure-temperature paths during hydrothermal alteration, S_1, S_2/S_3 and S_4 deformation (reaction boundaries from High Al-Pelites, Spear, 1993).

ica, and the support of the Department of Earth & Planetary Sciences at the University of New Mexico. We thank John Husler, SSU, retired staff chemist at the Department of E&PS, without whose expertise and gentle instruction, the geochemistry in this study would not have been possible.

REFERENCES

Aby, S.B., Karlstrom, K., Koning, D, and Kempter, K., 2010, Preliminary geologic map of the Las Tablas quadrangle, Rio Arriba County, New Mexico: N.M. Bureau of Geology and Mineral Resources, Open-file Geologic Map OF-GM-200, scale 1:12,000.

Afshooni, S.Z., Esmaelly, D., and Haroni, H.A., 2011, Mass changes during hydrothermal alteration/mineralization in Kahang exploration area (north eastern of Isfahan, central of Iran), EGU General Assembly 2011, Vienna, Austria: Geophysical Research Abstracts, v. 13.

Ague, J.J., 1994, Mass transfer during Barrovian metamorphism of pelites, south-central Connecticut. II: Channelized fluid flow and the growth of kyanite and staurolite: American Journal of Science, v. 294, n.1, p. 1061-1134.

Anderson, G.M., and Burnham, C.W., 1983, Feldspar solubility and the transport of aluminum under metamorphic conditions: American Journal of Science, v. 283-A, p. 283-29.

Barker, F., 1958, Precambrian and Tertiary geology of Las Tablas quadrangle, New Mexico: New Mexico Bureau of Mines and Mineral Resources Bulletin 45, p. 104.

Barrientos, X., and Selverstone, J., 1987, Metamorphosed soils as stratigraphic indicators in deformed terranes: An example from the Eastern Alps: Geology, v. 15, p. 841-844.

Bauer, P.W., and Williams, M.L., 1989, Stratigraphic nomenclature of Proterozoic rocks, northern New Mexico-revisions, redefinitions, and formalization: New Mexico Geology, v. 17, no. 33, p. 45-52.

Beach, A., 1976, The interrelations of fluid transport, deformation, geochemistry and heat flow in early Proterozoic shear zones in the Lewisian complex: Philosophical Transactions of the Royal Society of London, v. 280, p.569-604.

Bingler, E.C., 1965, Sillimanite group: Mineral and Water Resources of New Mexico, U.S. Congress, 89th, 1st session, Senate Committee, Interior and Insular Affairs, p. 298-299, 376-386.

Bonnet, A-L., and Corriveau, L., 2007, Alteration vectors to metamorphosed hydrothermal systems in gneissic terranes, *in* Goodfellow, W.D., ed., Mineral Deposits of Canada: A Synthesis of Major Deposit-Types, District Metallogeny, the Evolution of Geological Provinces, and Exploration Methods: Geological Association of Canada, Mineral Deposits Division, Special Publication No. 5, p. 1035-1049

Brown, A.J., Cudahy, T.J., and Walter, M.R., 2006, Hydrothermal alteration at the Panorama Formation, North Pole Dome, Pilbara Craton, Western Australia: Precambrian Research, v.151, p. 211–223.

Bowring, S.A., and Karlstrom, K.E., 1990, Growth, stabilization and reactivation of Proterozoic lithosphere in the southwestern United States: Geology, v. 18, p. 1203-1206.

Bronson, F.S., 1952, Fields of formation of some common hydrothermal alteration minerals: Economic Geology, v. 47, no. 6.

Bundy, W.M., 1958, Wall-rock alteration in the Cochiti Mining District, New Mexico: New Mexico Bureau of Mines and Mineral Resources, Bulletin

59, p. 71.
Burnham, C.W., 1962, Facies and types of hydrothermal alteration: Economic Geology, v. 57, p. 768-784.
Corey, A.F., 1960, Kyanite occurrences in the Petaca District, Rio Arriba County, New Mexico: New Mexico Bureau of Mines and Mineral Resources, Bulletin 47, p. 70 p.
Criss, R.E., and Champion, D.E., 1991, Oxygen isotope study of the fossil hydrothermal system in the Comstock Lode mining district, Nevada, *in* Taylor, H.P., O'Neal, J.R., Kaplan, I.R., eds., The Geochemical Society Special Publication No. 3, p. 437-447.
Deere, W.A., Howie, R.A., Zussman, J., 1997,Rock-forming minerals: Orthosilicates, The Geological Society, Alden Press, Oxford, UK., v.1a, 925 p.
Dipple, G.., and Ferry, J.F., 1992, Metasomatism and fluid flow in ductile fault zones: Contributions to Mineralogy and Petrology, v. 112, p. 149-164.
Dipple, G.M., Wintsch, R.P., and Andrews, M.S., 1990, Identification of the scales of differential element mobility in a ductile fault zone: Journal of Metamorphic Geology, v. 8, p. 645-661.
Feiss, P.J, Maybin, A.H., Riggs, S.R., and Grosz, A.E., 1991, Mineral resources of the Carolinas, *in* Horton, J.W., and Zullo, V.A., eds, The Geology of the Carolinas, Carolina Geological Society 50th anniversary edition: University of Tennessee Press, 1st edition, p 219-346.
Gall, Q., 1994, The Proterozoic Thelon paleosol, Northwest Territories, Canada: Precambrian Research, v. 68, p. 115-137.
Gammell, J.B., 2007, Hydrothermal alteration associated with the Gosowong Epithermal Au-Ag deposit, Halmahera, Indonesia: Mineralogy, geochemistry, and exploration implications: Economic Geology, v. 102; no. 5; p. 893-922.
Gay, A.L., and Grandstaff, D.E., 1980, Chemistry and mineralogy of Precambrian paleosols at Elliot Lake, Ontario, Canada: Precambrian Research, v. 12, p. 349-373.
Goff, F., and Gardner, J.N., 1994, Evolution of a mineralized geothermal system, Valles Caldera, New Mexico: Economic Geology, v. 89, p. 1803-1832.
Golani, P.R., 1989, Sillimanite-corundum deposits of Sonapahar, Meghalaya, India: a metamorphosed Precambrian paleosol: Precambrian Research, v. 43, p.175-189.
Grambling, J.A., Williams, M.L., Smith, R.F., and Mawer, C.K., 1989, The role of crustal extension in the metamorphism of Proterozoic rocks in northern New Mexico: *in* Grambling, J.A., and Tewksbury, B.J., eds., Proterozoic geology of the Southern Rocky Mountains: Geological Society of American Special Paper 235, p. 87-110.
Grandstaff, D.E., Edelman, M.J., Foster, R.W., Zbinden, E., and Kimberley, M.M., 1986, Chemistry and mineralogy of Precambrian paleosols at the base of the Dominion and Pongola Groups (Transvaal, South Africa): Precambrian Research, v. 32, p. 97-131.
Grant, J.A., 1986, The isocon diagram-A simple solution to Gresens' equation for metasomatic alteration: Economic Geology, v. 81, p. 1976-1982.
Grauptner, T., Kempe, U., Wall, V.J., Seltman, R., Kohler, S., and Shatov, V., 2005, Mass transfer during alteration and Au precipitation at Muruntau: Alteration behaviour of different rock types: Mineral Deposit Research: Meeting the Global Challenge, Session 12, Beijing, China, p.1317-1320.
Gresens, R.L., 1971, Application of hydrolysis equilibria to the genesis of pegmatite and kyanite deposits in northern New Mexico: Mountain Geologist, v. 8, p. 3-16.
Gresens, R.L., 1972, Staurolite-quartzite bands in kyanite quartzite at Big Rock, Rio Arriba County, New Mexico-A discussion: Contributions to Mineralogy and Petrology, v. 35, p. 193-199.
Gresens, R.L., 1976, Geologic, geochemical, and geochronologic investigation of Precambrian metamorphic rocks of the Las Tablas-La Madera quadrangles and the Picuris Range, northern New Mexico; a summary: New Mexico Geological Society Special Publication 6, p. 132-137.
Gresens, R.L., and Stensrud, H.L., 1974a, Geochemistry of muscovite from Precambrian metamorphic rocks of northern New Mexico: Geological Society of America Bulletin, v. 85, p. 1581-1594.
Gresens, R.L., and Stensrud, H.L., 1974b, Recognitions of more metarhyolite occurrences in northern New Mexico and a possible Precambrian stratigraphy: Mountain Geologist, v. 11, n. 3, p. 109-124.
Hemley, J.J. and Ellis, A., 1983, Geothermal systems ancient and modern: A geochemical review: Earth-Science Review, v. 19, p. 1-50.
Hobbs, B.E., Means, W.D., and Williams, P.F., 1976, An Outline of Structural Geology: New York, NY, John Wiley and Sons, 571 p.
Holland, H.D, Fakes, CR., and Zbinden, E.A., 1989, The Flin Flon paleosol and the composition of the atmosphere 1.8 BY: American Journal of Science, v. 289, p. 362-389.
Hurst, V.J., and Kunkle, A.C., 1985, Dehydroxylation, rehydroxylation, and stability of kaolinite: Clay and Clay Minerals, v. 33, no. 1, p. 1-14.
Kerrick, H.D., 1988, Al2SiO5 -bearing segregations in the Lepontine Alps, Switzerland: Aluminum mobility in metapelites: Geology, v. 16, p. 636-640.
Kimberley, M.M., and Grandstaff, D.E., 1986, Profiles of elemental concentrations in Precambrian paleosols on basaltic and granitic parent materials: Precambrian Research, v. 32, p. 133-154.
Klein, T.L., and Criss, R.E., 1988, An oxygen isotope and geochemical study of meteoric-hydrothermal systems at Pilot Mountain and selected other localities, Carolina Slate Belt: Economic Geology, v. 83, p. 801-821.
Krauskopf, K. B. and Bird, D.K., 1995, Introduction to Geochemistry, 3rd ed.: New York, McGraw-Hill, Inc., 647 pp.
Larson, T., 2003, Oxygen isotope analysis of aluminum silicate triple-point rocks in New Mexico and New Hampshire [PhD. Dissertation]: Albuquerque, University of New Mexico, 132 pages.
Lombardi, C.E., Williams, M.L., Breuninger, A.B., Karlstrom, K.E., 1996, Mushroom interference patterns, tectonometamorphic gradients, and regional correlation of fabrics and units, Proterozoic rocks, Tusas Mountains, New Mexico: Geological Society of America Abstracts with Programs.
Mao, J., and Bierlein, F.P., 2005, Mineral deposit research: meeting the global challenge: Proceedings of the 8th Biennial SGA Meeting, Beijing, China. v.1.
Meyer, C., and Hemley, J.J., 1967, Wall rock alteration, *in* Barnes, H.L., ed., Hydrothermal ore deposits: New York, NY, Holt, Rinehart, and Winston, Inc., p. 166-235.
Morton, R., Hudak, G., and Koopman, E., 1996, Physical volcanology, hydrothermal alteration and massive sulphide deposits of the Sturgeon Lake Caldera, Field Trip Guidebook B3: Geological Association of Canada/Mineralogical Association of Canada Annual Meeting, Winnipeg, Manitoba, May 27-29, 1996.
Newman, J., and Mitra, G., 1993, Lateral variation in mylonite zone thickness as influenced by fluid-rock interactions, Linville Falls fault, North Carolina: Journal of Structural Geology, v. 15, no. 7, p. 849-863.
Norman, D.K., Parry, W.T., and Bowman, J.R., 1991, Petrology and geochemistry of propylitic alteration at Southwest Tintic, Utah: Economic Geology, v. 86, no. 1, p. 13-28.
Pedrick, J. N., 1995, Polyphase Proterozoic tectonometamorphic history of the Taos Range, northern New Mexico, [Ph.D Dissertation]: Albuquerque, University of New Mexico. 146 p.
Pirajno, F., 2009, Hydrothermal Processes and Mineral Systems: New York, NY, Springer Press, 1250 p.
Reimer, T.O., 1986, Alumina-rich rocks from the early Precambrian of the Kaapvaal Craton as indicators of paleosols and as products of other decompositional reactions: Precambrian Research, v. 32, p. 155-179.
Retallack, G.J., 1986, The fossil record of soils, *in* Wright, P.V., ed, Paleosols: Their Recognition and Interpretation: Princeton, N.J., Princeton Univ. Press, p. 1-41.
Ring, U., 1999, Volume loss, fluid flow, and coaxial versus noncoaxial deformation in retrograde, amphibolite facies shear zones, northern Malawi, east-central Africa: Geological Society of America Bulletin, vol. 11, no. 1, p. 124-142.
Rose, A.W., and Burt, D.M., 1979, Hydrothermal alteration, *in* Barnes, H.L., ed., Geochemistry of hydrothermal ore deposits: Hoboken, N.J., John Wiley and Sons, p. 173-235.
Schmidt, R.G., Gumiel, P., and Pavas, A., 2006, Geology and mineral deposits of the Snow Camp-Saxapahaw Area, Central North Carolina: U.S. Geological Survey, Open-File Report 2006-1252, <http://pubs.usgs.gov/of/2006/1259/hydro_alt_min.html>.
Schreyer, W., and Chinner, G.A., 1966, Staurolite-quartzite bands in kyanite quartzite at Big Rock, Rio Arriba County, New Mexico: Contributions to Mineralogy and Petrology, v. 12, p. 223-244.
Selverstone, J., Mortenau, G., and Staude, J.M., 1991, Fluid channeling during ductile shearing: transformation of granodiorite into aluminous schist in the Tauern Window, Eastern Alps: Journal of Metamorphic Geology, v. 9, p. 419-431.
Simmons, M.C., 1999, Quartz-kyanite pods in Proterozoic rocks in northern New Mexico: Shear zone formation along an older hydrothermal alteration horizon, [M.S.thesis]: Albuquerque, University of New Mexico, 70 p.

Simmons, M.C., and Larson, T., 2001, Quartz-kyanite pods in Proterozoic rocks in northern New Mexico: Shear zone formation along an older hydrothermal alteration horizon: Abstracts with Programs - April 2001, v.33, issue 5, p. 44.

Smith, L.L., and Newcome, R., 1951, Geology of kyanite deposits at Henry Knob, South Carolina: Economic Geology, v. 46; no.7, p. 757-764.

Spear, F.S., 1993, Metamorphic phase equilibria and pressure-temperature-time paths: Washington, D.C., Mineralogical Society of America Monograph, 799 p.

Sykes, M. L.. and Moody, J. B., 1978, Pyrophyllite and metamorphism in the Carolina slate belt: American Mineralogist, v. 63, n. 1-2, p. 96-108.

VanBaalen, M.R., 1993, Titanium mobility in metamorphic systems: a review: Chemical Geology, v.110, p.233-249.

Warren, I., Simmons, S.F., and Mauk, J.L., 2007, Whole-rock geochemical techniques for evaluating hydrothermal alteration, mass changes and compositional gradients associated with epithermal Au-Ag mineralization: Economic Geology, v. 102, no. 5, p. 923-948.

Williams, M.L., 1990, Proterozoic geology of northern New Mexico: Recent advances and ongoing questions: N.M. Geological Society, 41st Field Conference Guidebook, p. 151-159.

Williams, M.L., 1991, Heterogeneous deformation in a ductile fold-thrust belt: The Proterozoic structural history of the Tusas Mountains, New Mexico: Geological Society of America Bulletin, v. 103, p. 171-188.

Williams, M.L., Karlstrom. K.E., Lanzirotti, A., Read, A.S., Bishop, J.L., Lombardi, C.E., Pedrick, J.L., and Wingsted, M.B., 1999, New Mexico middle-crustal cross sections: 1.65-Ga macroscopic geometry, 1.4-Ga thermal structure, and continued problems in understanding crustal evolution: Rocky Mountain Geology, v. 34, no.1, p. 53-66.

Winchester, J.A., 1984, Element mobility associated with syn-metamorphic shear zones near Scotchport, NM Mayo, Ireland: Journal of Metamorphic Geology, v.2, p. 1-11.

Wohletz, K. and Heiken, G., 1992, Volcanology and Geothermal Energy. Berkeley: Berkely, University of California Press, p. 432, <http:/lark.cdlib.org/ark3ll0 30/fr&19 pI 51I>.

APPENDIX 1. (a) Major & trace element analysis of various traverses.

Traverse 1	ss	q-k	q-k	q-k	q-k	q-k	q-k	q-k	q-k	q-k	q-k	ss	ss	rhy
	ms-107	K1.10	K1.9	K1.8	K1.7	K1.6	K1.5	K1.4	K1.3	K1.2	K1.1	ms-108	ms-52	ms-51
SiO_2	81.54	86.48	82.16	81.54	78.85	85.03	86.13	88.39	79.57	91.08	86.9	83.92	72.06	73.96
Al_2O_3	11.49	7.39	13.87	12.14	20.24	14.01	11.89	10.39	17.03	7.49	7.5	10.96	16.44	13.17
P_2O_3	0.03	0.05	0.04	0.04	0.04	0.04	0.05	0.04	0.04	0.06	0.04	0.03	0.05	0.04
CaO	0.07	0.09	0.05	0.07	0.06	0.06	0.06	0.06	0.06	0.07	0.08	0.06	0.22	0.31
TiO_2	0.11	0.09	0.14	0.1	0.17	0.19	0.13	0.11	0.12	0.09	0.08	0.1	0.26	0.13
$FeO+Fe_2O_3$	0.63	1.56	0	0.26	0.07	0.02	0.23	0.12	0.24	0.01	2.06	0	1.84	1.98
Na_2O	0.45	0.25	0.36	0.27	0.07	0.08	0.06	0.05	0.03	0.03	0.11	0.39	0.84	2.9
K_2O	2.93	2	0.88	1.4	0.24	0.14	0.11	0.15	0.19	0.24	0.83	2.69	4.54	4.12
MgO	0.08	0.25	0.05	0.07	0	0.04	0.07	0.24	0.04	0.1	0.1	0	0.29	0.17
MnO	0.02	0.02	0	0	0	0	0.01	0	0	0	0	0	0.01	0.02
H20 (-)	-	0.06	0	-0.08	0.02	-0.04	0.02	0	0.09	0.05	0.05	-	0.02	-0.08
LOI	-	1.16	0.89	1.40	0.52	0.38	0.65	0.43	0.41	0.46	0.97	-	2.38	1.32
TOTAL	97.35	99.4	98.44	97.21	100.28	99.95	99.28	99.98	97.82	99.68	98.72	98.15	98.95	98.04
						Trace Elements (ppm)								
Rb	85	68	20	37	8	5	3	4	5	9	22	52	140	117
Sr	13	11	9	8	4	3	5	3	5	4	5	45	19	31
Y	24	32	12	10	20	19	3	7	14	6	9	64	36	134
Zr	188	220	233	170	313	305	215	170	198	140	129	280	315	213
Nb	40	50	50	41	70	72	48	37	42	35	33	41	45	49

rhy = metarhyolite; ss = sericite schist; q-k = quartz-kyanite pod

APPENDIX 1 - cont.

Traverse 2	rhy	ss	rhy	rhy	ss	rhy	rhy
	ms-44	ms-39	ms-30	ms-35	ms-36a	ms-37	ms-38
SiO_2	73.45	78.19	75.59	76.56	68.38	76.12	74.4
Al_2O_3	15.43	12.17	13.16	11.9	17.45	11.61	13.23
P_2O_3	0.05	0.04	0.06	0.04	0.05	0.05	0.03
CaO	0.11	0.1	0.5	0.41	0.3	0.41	0.49
TiO_2	0.11	0.12	0.1	0.09	0.25	0.11	0.11
$FeO+Fe_2O_3$	1.97	1.96	1.39	1.23	3.03	1.54	1.5
Na_2O	0.39	0.28	2.51	2.5	1.04	3.48	3.68
K_2O	4.62	4.2	3.79	4.35	5.4	4.61	2.29
MgO	0.05	-	-	0.06	0.15	-	-
MnO	0.01	-	0.01	0.01	0.04	-	0.08
H20 (-)	0.10	0.10	0.10	0.11	0.14	0.02	0.08
LOI	2.52	1.15	1.28	1.41	3.02	0.42	1.80
TOTAL	98.81	98.31	98.49	98.67	99.25	98.37	97.69
			Trace Elements (ppm)				
Rb	210	128	183	204	210	111	137
Sr	17	63	55	36	31	46	8
Y	113	61	115	116	99	65	29
Zr	237	262	231	196	396	193	206
Nb	75	78	64	63	58	37	42

rhy = metarhyolite; ss = sericite schist

Traverse 3	rhy	ss	q-k	q-k	q-k	q-k	q-k	q-k	q-k	q-k	q-k	ss	rhy
	ms-109	ms-113	brk-9	brk-8a	brk-7	brk-6	brk-5	brk-4	brk-3	brk-2	brk-1	ms-114	ms-66
SiO_2	76.22	78.12	79.46	72.83	85.21	80.15	83.09	80.33	83.31	74.30	80.65	73.81	73.19
Al_{2O3}	11.84	14.41	16.62	24.41	13.01	16.92	13.87	16.21	12.87	22.24	14.66	17.37	13.03
P_2O_3	0.04	0.03	0.04	0.05	0.04	0.06	0.04	0.05	0.04	0.05	0.04	0.03	0.05
CaO	0.38	0.09	0.08	0.05	0.05	0.08	0.07	0.07	0.08	0.10	0.07	0.06	0.42
TiO_2	0.11	0.15	0.17	0.28	0.11	0.20	0.14	0.17	0.25	0.25	0.12	0.26	0.20
$FeO+Fe_2O_3$	1.50	-	2.23	-	-	-	-	-	-	-	-	0.22	2.60
Na_2O	3.00	0.81	0.16	0.06	0.17	0.08	0.11	0.08	0.10	0.05	0.40	0.45	2.35
K_2O	5.02	3.05	0.26	0.04	0.67	0.04	0.71	0.39	0.49	0.07	2.42	4.61	6.12
MgO	-	-	-	-	-	-	-	-	-	-	-	-	0.27
MnO	-	0.02	-	-	-	-	-	-	-	0.01	0.03	-	-
H_20 (-)	-0.06	0.72	0.05	0.08	-0.04	-0.06	0.93	0.63	0.61	0.41	1.62	0.05	0.08
LOI	1.64	2.26	0.69	0.48	0.55	0.56	0.00	-0.06	-0.04	-0.02	-0.02	2.54	0.83
TOTAL	99.69	99.66	99.76	98.28	99.77	98.03	98.96	97.87	97.71	97.46	99.99	99.40	99.14

APPENDIX 1 - cont.

	Trace Elements (ppm)												
Traverse 3	rhy	ss	q-k	q-k	q-k	q-k	q-k	q-k	q-k	q-k	q-k	ss	rhy
	ms-109	ms-113	brk-9	brk-8a	brk-7	brk-6	brk-5	brk-4	brk-3	brk-2	brk-1	ms-114	ms-66
Rb	18	88	14	2	22	1	24	15	22	3	76	153	175
Sr	35	32	7	3	8	5	4	4	5	5	18	13	36
Y	105	119	40	57	9	62	29	27	24	12	18	60	103
Zr	303	282	304	487	164	334	217	205	451	444	188	455	299
Nb	40	33	44	89	32	59	38	51	72	67	34	74	39

rhy = metarhyolite; ss = sericite schist; q-k = quartz-kyanite pod